日
米

U.S. - JAPAN COORDINATED PROGRAM FOR MASONRY BUILDING RESEARCH

REPORT NO. 2.4 (b) -1

Out-of-Plane Seismic Response of Reinforced Masonry Walls:

Correlation of Full-Scale Test and Analytical Model Results

by

Martin R. Button
Ronald L. Mayes

March 1991

supported by:

NATIONAL SCIENCE FOUNDATION
GRANT NOS. ECE-8518700 and BCS-8722866

COMPUTECH ENGINEERING SERVICES, INCORPORATED

CES

This report presents the results of a research project which was part of the U.S. Coordinated Program for Masonry Building Research. The program constitutes the United States part of the United States - Japan Coordinated Masonry Research Program conducted under the auspices of the Panel on Wind and Seismic Effects of the U.S.-Japan Natural Resources Development Program (UJNR).

This material is based on work supported by the National Science Foundation under the direction of Program Director, Dr. S.C. Liu.

Any opinions, findings, and conclusions or recommendations expressed in this publication are those of the authors and do not necessarily reflect the views of the National Science Foundation and/or the United States Government.

U.S. - Japan Coordinated Program for Masonry Building Research

Report Number 2.4 (b) - 1

Out-of-Plane Seismic Response of Reinforced Masonry Walls: Correlation of Full-Scale Test and Analytical Model Results

by

Martin R. Button
and
Ronald L. Mayes

Computech Engineering Services
2855 Telegraph Ave, Suite 410
Berkeley, CA 94705

March 1991

supported by:

The National Science Foundation
Grant Nos. ECE-8518700 and BCS-8722866

ib

Abstract

An analytical model is developed to predict the out-of-plane seismic behavior of reinforced masonry walls. The formulation and implementation of the model are described. Results for global responses (deflections, moments and reactions) from the model are compared to those obtained from full-scale dynamic test programs on nine clay brick walls and four concrete block walls. The test walls cover a typical range of key wall parameters (H/t ratio, vertical reinforcing, splices, grouting and vertical load). It is concluded that the analytical model captures the global wall response well, over the range of wall parameters included in the tests. A subsequent report will use the model developed and verified here to extend the range of wall parameters studied during the test programs.

Acknowledgements

This work was funded by grants ECE-8518700 and BCS-8722866 from the National Science Foundation. This support is gratefully acknowledged. Marcial Blondet and Trevor Kelly provided helpful comments at various stages of the project. Judy Peterson produced the manuscript.

Out-of-Plane Seismic Response of Reinforced Clay Brick Walls: Correlation of Full-Scale Test and Analytical Model Results

Table of Contents

1 Introduction

This report describes the development and correlation of an analytical model to predict the out-of-plane seismic response of reinforced masonry walls. The work is Task 2.4(b) of the U.S. part of the U.S.-Japan Coordinated Program for Masonry Building Research.

The analytical model is contained in a stand-alone computer program, **WALLY**, which can be used for the analysis of the out-of-plane seismic response of masonry walls of arbitrary configuration. An appendix to this report describes the use of this program.

The analytical model is verified by comparing its predicted response with that measured during two full-scale dynamic test programs. The first program [1,2] subjected each of nine clay brick walls to at least 12 seismic motions of steadily increasing severity. The second program [3] made less extensive dynamic tests on reinforced concrete block walls. Results for deflections, moments and forces from the analytical model are correlated with corresponding results from these programs to develop a high degree of confidence in the model. A series of static air bag tests on concrete block walls [4] are also used to understand wall behavior.

There are two equally important reasons for developing the analytical capabilities described in this report. The first is to enable designers to get a feel for the realistic response of out-of-plane walls, and thus improve the serviceability and safety of walls in their designs. The second is to use the verified model to expand the scope of parameters explicitly studied during the test programs. This expanded set of wall responses will be invaluable for the development and evaluation of code design procedures for reinforced masonry walls. This report focuses solely on the correlation of analytical and test responses. A forthcoming accompanying report describes the results of the parameter studies using the validated model.

To set the stage, Section 2 of this report briefly describes the behavior of the walls during the clay brick test program. Key parameters influencing wall response are identified. Section 3 discusses the formulation and development of the analytical model, including detailed descriptions of the hysteretic behavior of the model. The detailed correlation between analytical results and test results is described for a limited number of test walls in Section 4 of the report. Summary correlations are provided for the remaining walls in the clay brick program and for selected concrete block test walls. Conclusions are drawn in Section 5.

2 Behavior of Test Walls

This section provides a brief description of the clay brick test program, followed by some observations on the overall behavior of the walls. A good summary of the behavior of the 25 foot walls may be found in [5].

Nine full-scale clay brick masonry walls (two with a height of 20 feet, seven with a height of 25 feet) were tested dynamically under Task 3.2(b2) of The Coordinating Committee for MAsonry Research (TCCMAR). The walls were 4 feet wide, constructed with nominal 6"x4"x16" hollow clay bricks, with an actual thickness of 5.5".

The physical properties for the nine dynamic walls are shown schematically in Figure 1 and are listed as follows (walls 1 and 2 were tested using static cycling):

Wall No.	Height (feet)	Nominal H/t	Vertical Rebar	Vertical Load (lb/ft)	Lap Splices	Grouting
3	25	50	3 #7	800	No	Full
4	20	40	2 #5	50	No	Full
5	25	50	3 #7	800	No	Full
6	20	40	2 #5	300	No	Full
7	25	50	3 #7	300	No	Full
8	25	50	3 #7	300	No	Partial
9	25	50	2 #5	300	Yes	Partial
10	25	50	3 #7	300	Yes	Partial
11	25	50	3 #7	300	Yes	Partial

The walls were in turn placed on a shake table with one horizontal degree of freedom, and excited independently at the top and bottom with displacement controlled servo-hydraulic actuators. Instrumentation varied slightly from wall to wall, but a typical wall had 11 horizontal displacements, 11 horizontal accelerations, 12 joint deformations and 15 rebar strains measured during each dynamic run.

A series of displacement time histories were generated to simulate ground motions representative of various seismic regions in the United States. Four records had an effective peak acceleration (EPA) of 0.1g, two had an EPA of 0.2g, four had an EPA of 0.4g and two had an EPA of 0.8g. All records conformed closely to the ATC S1 spectral shape for the given EPA level. This sequence of 12 motions was used on all walls (some walls were

subjected to additional shaking). The excitation at the base of the walls corresponded to each earthquake ground motion, while the input at the top was analytically computed to represent the corresponding response at the roof level of a typical warehouse structure.

2.1 General Observations

No visible evidence of damage was apparent for any of the 25 foot walls up to and including the 0.4g EPA S1 tests. However, considerable softening of each wall from its initial uncracked state had occurred during these tests. This was apparent by plotting the computed midheight moment against the observed midheight deflection and noticing the shape of the resulting hysteresis loops. Such a plot for wall 9 during the first 0.1g run is shown in Figure 2.

Typical midheight deflections expressed as a ratio of wall height were 0.002 to 0.003 for the 0.1g EPA S1 tests, 0.006 to 0.008 for the 0.2g tests and 0.017 to 0.023 for the 0.4g tests. As noted above, these levels of deflection are readily sustainable by well constructed masonry walls.

Visible damage was not apparent in any of the walls until the 0.8g EPA S1 tests. At this point, joint cracking was evident to the naked eye, and permanent offsets remained at the conclusion of shaking. Recorded rebar strains indicated that yielding of the vertical steel had occurred, and the moment hysteresis loops took on a new shape. Such a loop for wall 10 during the first 0.8g EPA S1 test is shown in Figure 3. After yield of vertical steel, the walls exhibit a slight negative stiffness at low amplitudes, with a recovering positive stiffness at larger deflections. This complete loss of stiffness is caused by permanent rebar extension at several joints, combined with faceshell openings on either side of the bricks. The negative stiffness is due to the destabilizing effect of the compressive vertical load. This effect is always present, but becomes apparent only when the mechanical stiffness of the wall becomes negligible. Positive stiffness does not occur until the faceshell opening on one side of the wall completely closes. This is discussed further in Section 3.

Typical midheight deflections expressed as a ratio of wall height during the 0.8g EPA S1 tests were 0.040 to 0.060 (12" to 18" for the 25 foot walls). Although permanent offsets were noted at the conclusion of the these tests (of the order of 4" to 6"), the walls were capable of supporting their own weight and the ledger load.

2.2 Key Parameters

Deflection ratios for the two walls with an H/t ratio of 40 are similar at all levels of shaking to the corresponding ratios for the walls with an H/t of 50. However, the shorter walls have a much higher uncracked stiffness, and thus the H/t ratio may be an important parameter at low levels of shaking.

The amount of vertical steel in the wall is an important parameter. As the reinforcement ratio increases, the cracked stiffness becomes larger, and the stiffer wall attracts larger

inertia forces, and thus bending moments. The wall tests indicated that the overall deflections were similar for the two levels of reinforcement ($0.16\rho_b$ and $0.50\rho_b$). However, this similarity did not occur at the local level: walls with lower steel content tended to have slightly larger rebar strains and faceshell openings.

Stiffness degradation during low intensity runs was delayed in walls with lap splices as compared to similar walls without splices. The bond beams associated with the splices allowed the rebar to develop its strength, and thus the effective cracked stiffness in spliced walls was increased. The effect of splices decreased rapidly as the level of shaking increased.

The effect of grouting was similar to that of splices. Walls that were fully grouted tended to have lower response during low intensity runs than partially grouted walls. After yielding and loss of stiffness at low displacements, the increased weight of the fully grouted walls tended to induce larger deflections than observed in their partially grouted counterparts.

The vertical ledger load appeared to have a significant influence on the deflection response of the walls: those with higher vertical load responded significantly less than corresponding walls with low ledger loads. The vertical load thus appears to have two seemingly opposite effects: it has a destabilizing influence as seen with the negative stiffness at low displacements after yield, yet higher compressive loads apparently tend to decrease deflections.

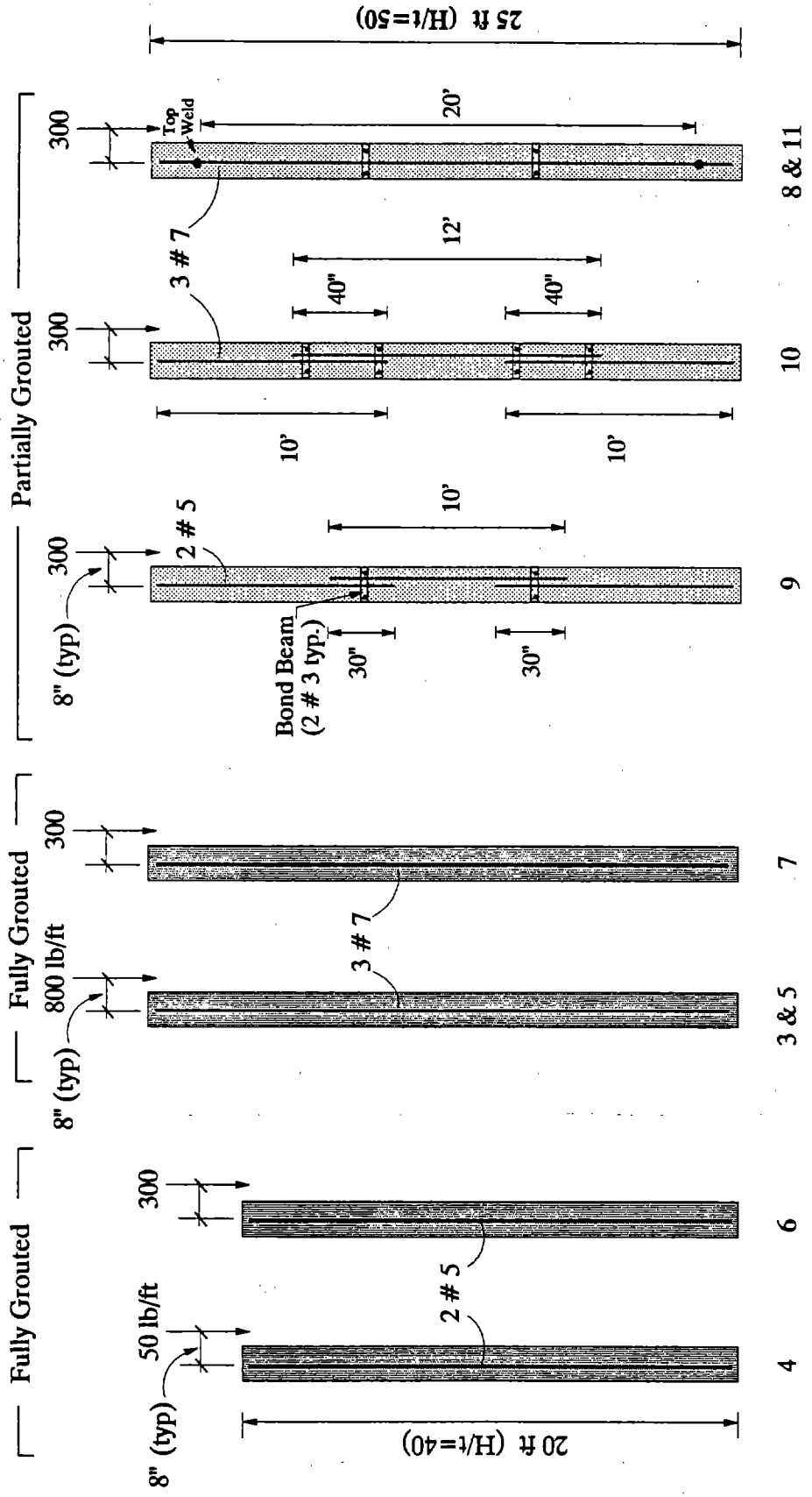

Figure 1: Characteristics of Test Walls

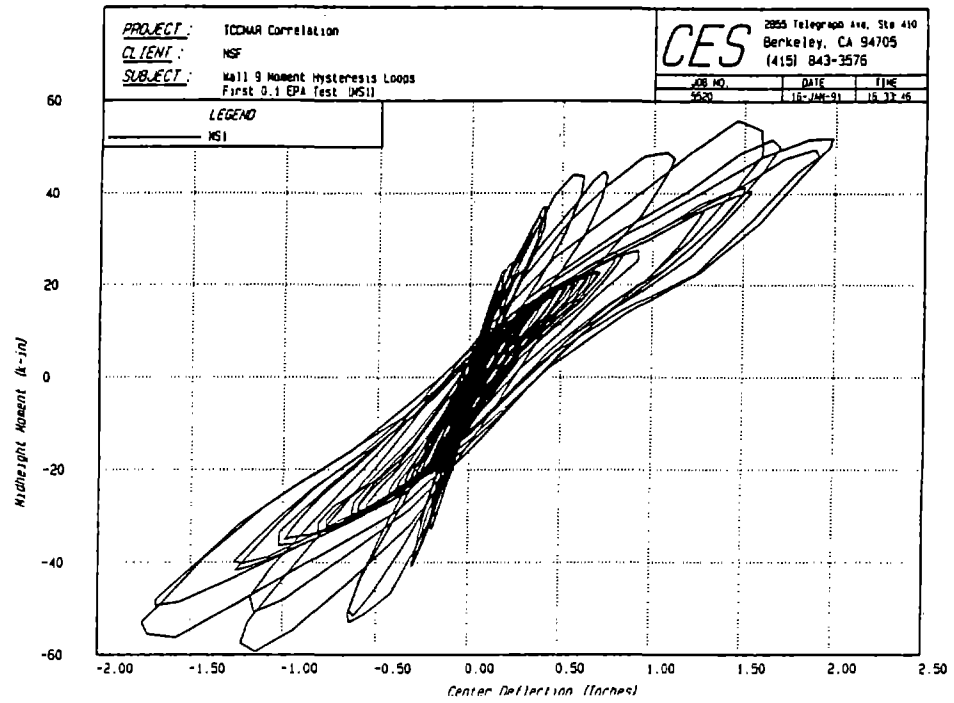

Figure 2: Wall 9 Moment Hystersis Loops for 0.1 EPA Test

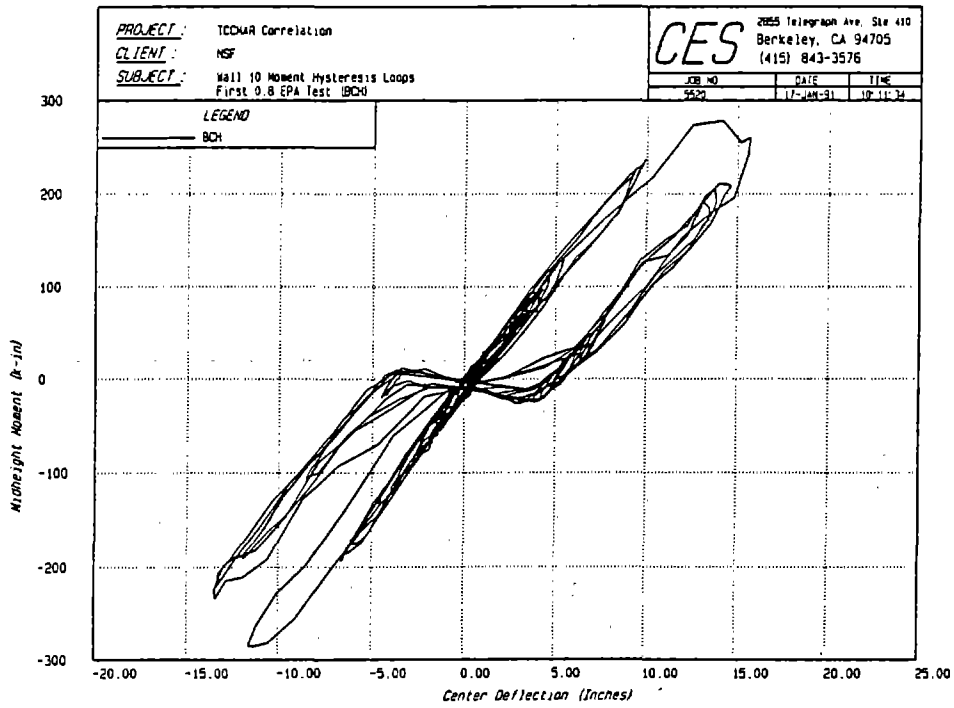

Figure 3: Wall 10 Moment Hystersis Loops for 0.8 EPA Test

3 Description of Analytical Model

This section provides a detailed description of the mathematical representation of the dynamic out-of-plane behavior of reinforced masonry walls. The section starts with a review of overall wall behavior observed during the tests, and proceeds to develop a mathematical model to represent this behavior. The model described here is a "structural component model" (SCM) which is intended to directly predict the global response (maximum moments, forces and deflections) of a wall. It is not intended to directly provide any information on the details of local response (faceshell strains and rebar strains).

3.1 Review of Wall Behavior

The overall wall behavior was briefly described in Section 2.1. Referring to Figures 2 and 3, we note that the wall behavior is amplitude dependent and thus highly non-linear. However, the behavior can be divided into three major phases.

The first phase occurs at very low levels of response, when at every location in the wall, the applied moment is less than the corresponding cracking moment. We note here that due to variations in the mortar modulus of rupture (f_r) from one joint to the next, the cracking moment is a (random) function of position within the wall. During this phase, the response is linear elastic with essentially no hysteretic area, and thus no hysteretic damping.

The second phase begins once the first joint in the wall cracks, and continues until there is generalized yielding of the vertical steel at one or more joints. We note here that the first joint to crack will not necessarily be at the location of maximum applied moment, due to the variation in the mortar modulus of rupture. However, the most highly stressed joint is the most likely to crack first. During this phase, the response is characterized by a series of degrading elastic stiffnesses, with some hysteretic area apparent. Each elastic stiffness is maintained until the previous maximum deflection is exceeded, when the wall stiffness degrades to a new stiffness consistent with the new maximum deflection. A moment exceeding the previous maximum moment is required to degrade the stiffness since previously uncracked joints must be cracked. Thus, physically, this phase is characterized by an increasing number of cracked joints within the wall height. While no further joints crack, the effective stiffness remains essentially constant. Local deformations in the cracked joints provide the hysteretic area. We also note here, that near the beginning of this phase of the response, the wall may have unequal stiffnesses for deflections of opposite signs, since an unequal number of joints may be cracked on opposite faces of the wall. After the very first cracking excursion, one face will have one or more cracked joints, while the opposite face remains intact. This is demonstrated in Figure 4. Eventually, a sufficient number of joints will crack on each side of the wall that any difference in stiffness for the two directions becomes negligible.

The third phase begins once there is generalized yielding of the vertical steel. In this context generalized yielding is taken to mean that there is inelastic elongation of the reinforcing bar, as opposed to localized yielding over a small part of the cross section. At the start of this phase, the effective stiffness of the wall is very close to that corresponding to the fully cracked section. Suppose that generalized yielding occurs at just one joint. At that joint, one faceshell is in compression, the central rebar stretches inelastically, and the opposite faceshell opens. Upon load reversal, the compression faceshell unloads at the fully cracked section stiffness, until that faceshell just begins to open at the joint. At this stage, the wall has no mechanical stiffness at that joint, except the negligible flexural stiffness of the reinforcing steel. This zero stiffness state continues until the opposite faceshell comes into contact (at a deflection equal but opposite to that when the first faceshell opened). From there, the wall regains mechanical stiffness, again equal to the fully cracked stiffness. This mechanism is shown schematically in Figure 5, and the resulting hysteresis loops are shown in Figures 3 and 6. Again the loops have some hysteretic area due to local deformations in the cracked joints. The loops are stable until the previous maximum deflection is reached, when the rebar will further plastically elongate, and the range of deflections with zero mechanical stiffness will increase. This behavior is clearly apparent in wall 10 as shown in Figure 6. A stable series of loops has occurred with a maximum deflection of about 13 inches, and a limit for zero stiffness of about 4 inches. After an excursion to 17 inches, the limit for zero stiffness is increased to about 6 inches, and a new stable regime is observed.

Thus the wall behavior may be briefly summarized in the following phases:

1. Linear elastic, uncracked stiffness.
2. Cracked, with linear degrading stiffness.
3. Yielded, with either zero stiffness or fully cracked stiffness.

3.2 Overview of Model

The model consists of a number of inelastic beam-column elements arranged vertically to represent a particular wall. Each element is a series combination of an elastic flexural line element with an inelastic hinge at each end. It is not predetermined where within the wall height the inelastic hinge will form (i.e. between which elements) but for numerical stability, once one hinge forms, no other hinges are permitted. (This, of course, does not preclude the formation of a base hinge in a fixed base wall.) This arrangement is shown in Figure 7.

The model is implemented in a stand-alone computer program, which runs on an IBM PC or compatible, requiring 640k RAM and a color graphics monitor. The program is based on the ANSR-II code [6], but is highly specialized for out-of-plane wall analysis in three ways: first, the program is specialized from a general three-dimensional formulation to a two-dimensional one — this speeds up run time considerably; second, the program contains elements specifically developed to model out-of-plane walls; and third, the program input and output is masonry wall specific. The program is user-friendly, accepting input in either interactive or batch mode, and has analysis results available to the user through an on-screen graphics processor at the conclusion of computations.

The non-linearities in a typical wall are distributed over a good proportion of the wall's height — in fact they arise at each joint in the wall which suffers cracking. The analytical model will typically consist of six flexural elements over the wall height, and for a 25 foot wall, each element represents about 4 feet of wall height (6 to 12 joints). Thus it is inevitable that the individual non-linearities at each joint will not be **explicitly** represented in such a model. For reasons of numerical stability, we further restrict the model non-linearities to a single location within the wall height. As mentioned above, the location of this point is not pre-determined (it will typically occur at the midheight of the wall, although it may occur elsewhere in cases with vastly different intensities of shaking at top and base of the wall).

The task of developing the inelastic flexural element then becomes one of defining the appropriate properties of a single inelastic hinge which will adequately represent the distributed non-linearities observed during wall testing. The properties of the hinge must allow wall response in each of the three major phases previously identified. It is worth noting here that the analytical inelastic hinge is not the same as a physical plastic hinge — it is merely a convenient way of introducing a specific shape of hysteresis loop to a flexural element through a moment-rotation relationship at a point. The flexural stiffness of the element is then a series combination of the elastic stiffness of the line element and the current moment-rotation stiffness of each of the two end hinges.

The overall distributed non-linearities observed during the wall testing have been used as the basis to determine the lumped non-linearities associated with the inelastic hinges. The specifics of the hinge behavior are described in Sections 3.3 and 3.4. These sections typically refer to deflections rather than rotations. The hinge moment-rotation properties are computed so that the hinge stiffnesses, when combined with the elastic stiffness of the line elements, will give the overall moment-deflection hysteresis loops discussed in the following sections.

3.3 Hysteretic Behavior Pre-Yield

This section describes the hysteretic behavior of the model during the first (uncracked) and second (cracked but not yielded) phases of response.

Several quantities are computed prior to the beginning of the analysis, as follows (refer to Figure 8).

Cracking Moment, M_{cr} — This is computed using the uncracked section modulus and the mortar modulus of rupture. A value lower than the mean modulus of rupture should be used since the first crack to form is of interest.

Yield Moment, M_y — This is computed in the normal fashion using a mean value for the yield stress of steel. This will typically be somewhat higher than the design nominal value.

Hysteretic Moment, M_o — This is determined empirically as a fraction of the cracking moment. From the test data, a value of 25% of the cracking moment is reasonable. The moment hysteresis loops pass through $\pm M_o$ at zero deflection.

Cracking Deflection, Δ_{cr} — This is computed from the cracking moment and the uncracked section properties of the wall. Young's modulus is taken as $500f'_m$ for clay brick. A uniform distribution of load is assumed.

Yield Deflection, Δ_y — This is computed from the cracking moment, the yield moment and the cracked and uncracked section properties of the wall. A uniform distribution of load is assumed.

Initially the wall is uncracked and elastic, and its stiffness is represented by the elastic flexural stiffness of the line elements. Thus the initial stiffness of the moment rotation hinges is set several orders of magnitude larger than the end rotational stiffness of the elastic line element. Thus all the deformation in the model during this phase of response is flexural deformation of the line elements at the uncracked stiffness.

Once the cracking moment is exceeded anywhere in the analytical model, the response shifts to phase 2, and the inelastic hinges are activated. At this point it is instructive to examine Figure 9, a composite moment hysteresis plot for all wall 10 runs up to and including the 0.4g EPA S1 tests. The wall does not yield during these runs. Also shown on this plot are lines connecting the cracking point and the yield point as computed above — in effect we are overlaying Figure 8 and the experimental plot in Figure 9. It can be clearly seen that these lines represent the hysteresis envelope, and excursions beyond the previous maxima closely follow these lines, which will be referred to as the virgin curve.

Once the cracking moment is exceeded in the analytical model, an inelastic hinge forms at the point where the cracking moment was first exceeded. The hinge stiffness is such that the overall moment deflection trace follows the virgin curve. The point of unloading defines the new "secant" wall stiffness as follows (refer to Figure 10). Suppose that unloading occurs at point A. A line AB through $+M_o$ is constructed, and also a parallel line CD through $-M_o$. Note that point C is directly opposite point A on the other branch of the virgin curve. The unloading stiffness AE is degraded as a quadratic function of displacement, from the uncracked stiffness at point X (at the cracking displacement) to twice the fully cracked stiffness at point Y (the yield displacement). This degradation is empirically based, and the overall response is not particularly sensitive to it. If CH is drawn parallel to AE, then the parallelogram AECHA represents the current hysteresis loop until point A or C is exceeded.

However, unloading does not follow AEC until an "equal stiffness" criteria for positive and negative deflections has been met. Physically, after the first cracking excursion with positive deflection, the wall will still be uncracked on the opposite face. Thus, the path from A is AEFGC, following the uncracked virgin curve FG on the opposite side, until that face also cracks.

During the early stages of response, the numbers of cracked joints on opposite faces of the wall are unequal. In this case the "secant stiffness" is different for positive and negative deflections. The two stiffnesses and their associated hysteretic areas are defined as described above (as shown in Figure 10), based on the maximum positive and negative deflections. The resulting hysteresis loop is ABCDEFA in Figure 11. The shape of the loop changes as the maximum deflections A and D change. It should be noted here that paths AB and DE are reversible, whereas a load reversal from any other part of the loop is irreversible, and occurs with a stiffness parallel to AB or DE (depending on the sign of the deflection).

Once there have been at least two independent excursions on the post-cracked virgin curve for both positive and negative deflections, or once 10% of the yield deflection has been reached on any one side, unequal secant stiffnesses for positive and negative deflections no longer apply. These criteria are based on observations of experimental hysteresis loops. With reference to Figure 11, if a deflection to point G satisfies one of the "equal stiffness" criteria, then the subsequent path will be GHFI rather than GHFA which would be the case if the equal stiffness criteria were not yet met. The current hysteresis loop is thus the parallelogram GHFIJCG. Again, the stiffness of this loop is determined by the current maximum absolute deflection.

Once the equal stiffness criteria are met, the element contains an ability to degrade the width of the hysteresis loops if reversals occur prior to the maximum deflection associated with the loop. This behavior is described with reference to Figure 12. The current hysteresis loop is ABCDEFA. Suppose a load reversal occurs at point G. Then the subsequent load path is GHIJ, which intercepts the moment axis (point I) at a point other than $-M_0$ (point C). If point O is the origin, point I is chosen so that the ratio OI/OC is equal to the ratio Δ_G/Δ_A. The width of the hysteresis loop is returned to its full value ($2M_0$) when point A or D is exceeded. This feature of the element recognizes the loss of hysteretic damping at small amplitudes following larger cycles.

One final feature of the pre-yield hysteretic capabilities of the element is the ability to start an analysis assuming a wall has already undergone some shaking and associated softening. This is achieved by specifying the previous maximum deflection that the wall has experienced. Initial response is computed using a stiffness based on the original virgin curve and the previous maximum deflection, as indicated in Figure 13. Essentially this amounts to a modification of the virgin curve, with the initial stiffness changed from that based on the uncracked section, to that described above. Currently, no hysteretic effects are included in this case, until the response exceeds the previous maximum.

The model's behavior before yield is thus essentially a degrading stiffness with a relatively narrow hysteretic area. The specific rules describing the hysteretic behavior are based on observed response of the test walls [1,2,3,4,5,9].

3.4 Hysteretic Behavior Post-Yield

This section describes the hysteretic behavior of the model during the post-yield phase of response. As noted earlier, the wall behavior after generalized yielding occurs is quite different to its pre-yield behavior. This difference is most pronounced in a region where the wall has essentially no mechanical stiffness at low deflections. The associated physical mechanism was described previously.

The basic post-yield hysteretic loop is shown in Figure 14. It is constructed as follows. The virgin curve is extended horizontally from both the positive and negative yield points. The model begins its post-yield behavior as it reaches point A at the yield deflection. At this point, the line OA defines the basic post yield stiffness, which is very close to the stiffness based on the fully cracked section. The wall continues a yielding excursion along the virgin curve to point B, where the load reverses. A pair of lines DE and HI are constructed parallel to AB through $-M_0$ and $+M_0$ respectively. From point B, a line BI is constructed parallel to OA, and point D is established vertically below point I. An initial unloading stiffness based on $2I_{cr}$ establishes point C, with CD parallel to BI. From the point of load reversal (point B) the path is thus BCDE, with DE representing the region of no mechanical stiffness. At point E (directly opposite point I) the model stiffens, corresponding to the physical closing of the faceshell gap on the tension side of the wall at point B. The stiffness EF is identical to CD, with point F diametrically opposed to point B. The path from F to B (FGHIB) is constructed identically to that from B to F. The basic post yield loop is thus BCDEFGHIB, which is stable while the absolute deflections are less than that at B. Load reversal on BC or FG occurs at the same stiffness, while load reversal anywhere else in the loop occurs with a stiffness equal to that of BC or FG. When the loop maximum deflection is exceeded, travel is along the virgin curve, for example from B to P. A load reversal at point P establishes a new stable loop, constructed exactly as described previously, but having a larger range of deflections for which there is no mechanical stiffness. No degradation of hysteretic width occurs after yielding.

The model's behavior after yielding is thus amplitude dependent: at low amplitudes, the model has no mechanical stiffness, while at larger amplitudes, the model exhibits a stiffness approximately equal to the fully cracked stiffness. The range of deflections over which zero stiffness occurs increases as the maximum post-yield deflection increases. A relatively narrow hysteretic area is maintained. This behavior is completely consistent with observed wall behavior (see, for example, Figure 6).

3.5 Excitation of Model

The model is excited by two motion histories — one applied at the base support of the wall, the other at the top. The effective external load vector at each time step is computed from the support displacements. Details of this technique are described in [7]. Support motions may be input to the program in the form of displacement, velocity or acceleration histories. If velocity or acceleration histories are used, they will be integrated by the program to obtain displacement histories prior to the start of step-by-step analysis. These histories must be

defined with sufficient precision at a sufficiently fine time step to enable integration to displacement histories to be performed meaningfully.

The base motion will typically be a ground motion representative of the seismicity and soil conditions at the site of the structure containing the wall. The top motion should be computed using an analytical model of this structure. This model should be excited by the above ground motion, and the response at the location of the top of the wall should be computed. If an acceleration history is computed, it must be absolute and not relative acceleration.

Since the computation of the top motion is performed using a model that will typically not contain the out-of-plane walls, structural interaction between the wall and the rest of the structure will not be included in the computed motions. If significant interaction is a possibility, then care must be taken to include it in the computation of the top support motion. This would typically be done by including a linearized model of the out-of-plane wall stiffness in the overall structural model. Judgement needs to be exercised here in deciding on the appropriate stiffness for the out-of-plane walls, since in reality, this is amplitude dependent. An iterative scheme may be necessary to arrive at an appropriate top motion. Using the hysteretic properties described previously, it is straightforward to determine an appropriate equivalent stiffness for a wall for any level of deflection. The iteration would consist of guessing a level of wall response, computing the top motion from a structural model containing the corresponding wall stiffness, and finally computing the wall response using the non-linear program. The computed level of wall response would be checked against the initial assumption, and the process repeated using the computed response as a starting point, until reasonable convergence was obtained.

It is intended to include the non-linear model for out-of-plane masonry walls developed here in the LPM program [8] for the analysis of a full building. Once such an inclusion is made, any interaction between out-of-plane walls and the rest of the structure will be modelled explicitly, and the above iterative approach will become unnecessary.

3.6 Hysteretic and Viscous Damping

The model contains both hysteretic and viscous damping. The hysteretic damping is explicitly represented in the form of the moment-rotation relationship for the inelastic hinges. Viscous damping is user-specified as a fraction of critical damping. Values of user-specified viscous damping necessary to obtain good correlation with test results are typically around 1% of critical.

Using techniques discussed in [7], the equivalent viscous damping from the hysteretic action of the inelastic hinges has been computed as a function of the maximum midheight deflection in the wall. The results of these computations are conveniently expressed in non-dimensional plots such as Figure 15. The deflection ratio on the horizontal axis is defined as $(\Delta_{max} - \Delta_{cr}) / (\Delta_y - \Delta_{cr})$. Below yield, this ratio ranges from 0.0 to 1.0. It is noted that the equivalent viscous damping rapidly increases from zero when Δ_{max} equals Δ_{cr}, to a maximum when the maximum deflection is about 5% to 10% of the yield deflection. For

the curves shown, the maximum equivalent damping is between 10% and 12% of critical. Once the deflection increases, the equivalent viscous damping drops to between 3% and 6% near the yield deflection. Very similar values for equivalent damping are obtained when the parameters in these non-dimensional plots are varied over a practical range.

It is worth noting here that the equivalent damping associated with peaks of the curves should not be used as a design value. The curves are developed assuming that the hysteretic width is full. As explained previously, loops at deflections corresponding to the peaks in these curves, occurring after larger amplitude cycles, will have a lesser hysteretic width and correspondingly lower equivalent damping. For wall responses approaching the yield deflection, then, reasonable values of hysteretic damping suggested by this analysis are in the range of 3% to 6%. When the (approximately) 1% viscous damping which must be user-supplied to obtain good correlation with test results is considered, then the appropriate total equivalent damping is in the 4% to 7% range. Since the analytical hysteresis loops were closely modelled on the test loops, these figures represent reasonable values for damping in out-of-plane reinforced walls.

3.7 Geometric Stiffness

In viewing Figures 3 and 6 (moment hysteresis loops) and especially Figure 16 (inertia force hysteresis), the destabilizing effect of the self weight of the wall and the applied ledger load is clearly visible. This effect is accounted for in the model by including geometric stiffness in the formulation. This approach is adopted rather than using a large displacement formulation in order to improve computational efficiency without significant loss in accuracy. However, because of this approach, the negative stiffness at low deflections after yielding shows up in the model only in the reaction-deflection hysteresis loops. The model moment-deflection loops show zero stiffness at small deflections.

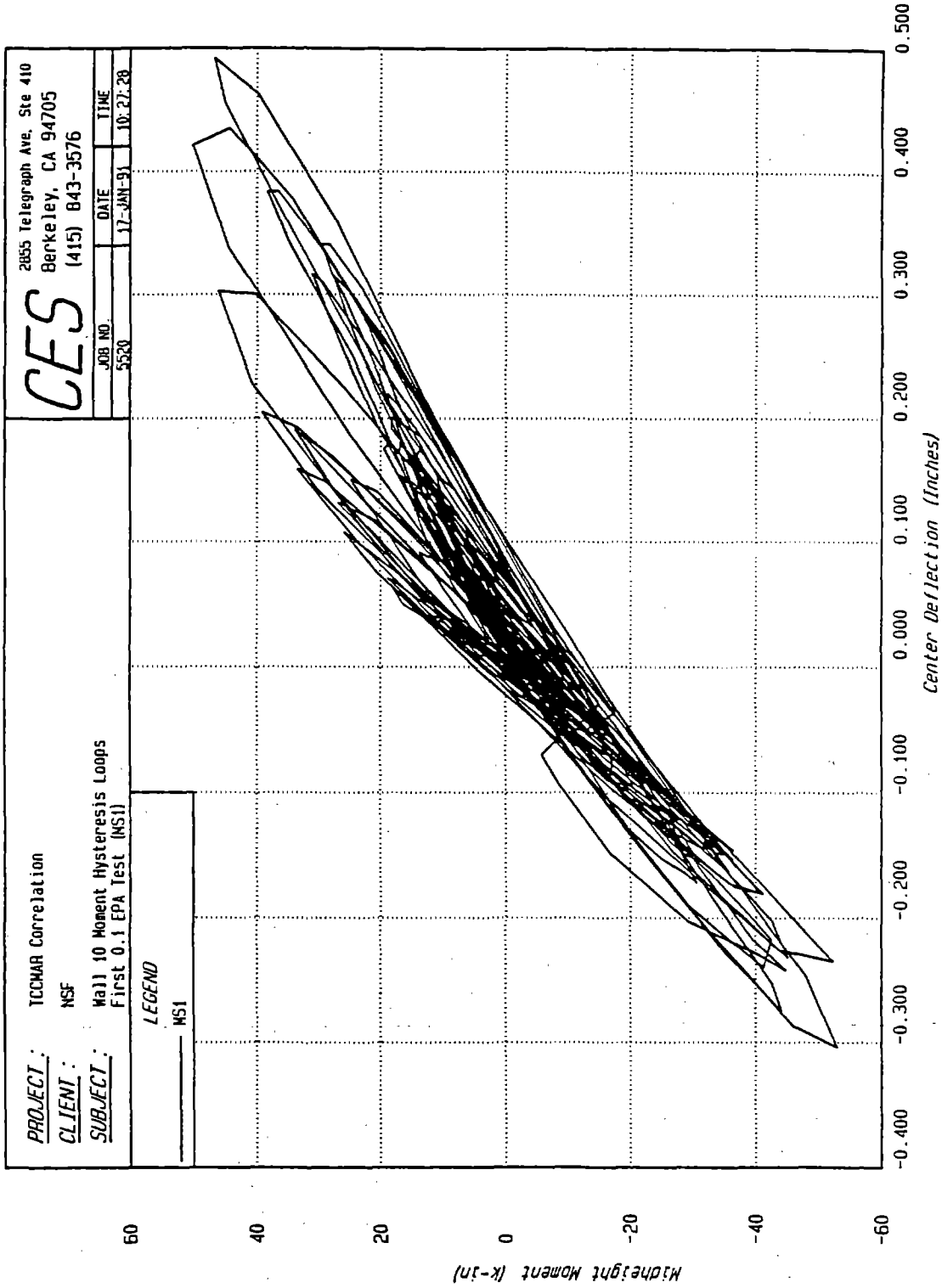

Figure 4: Unequal Stiffness for Positive and Negative Deflections

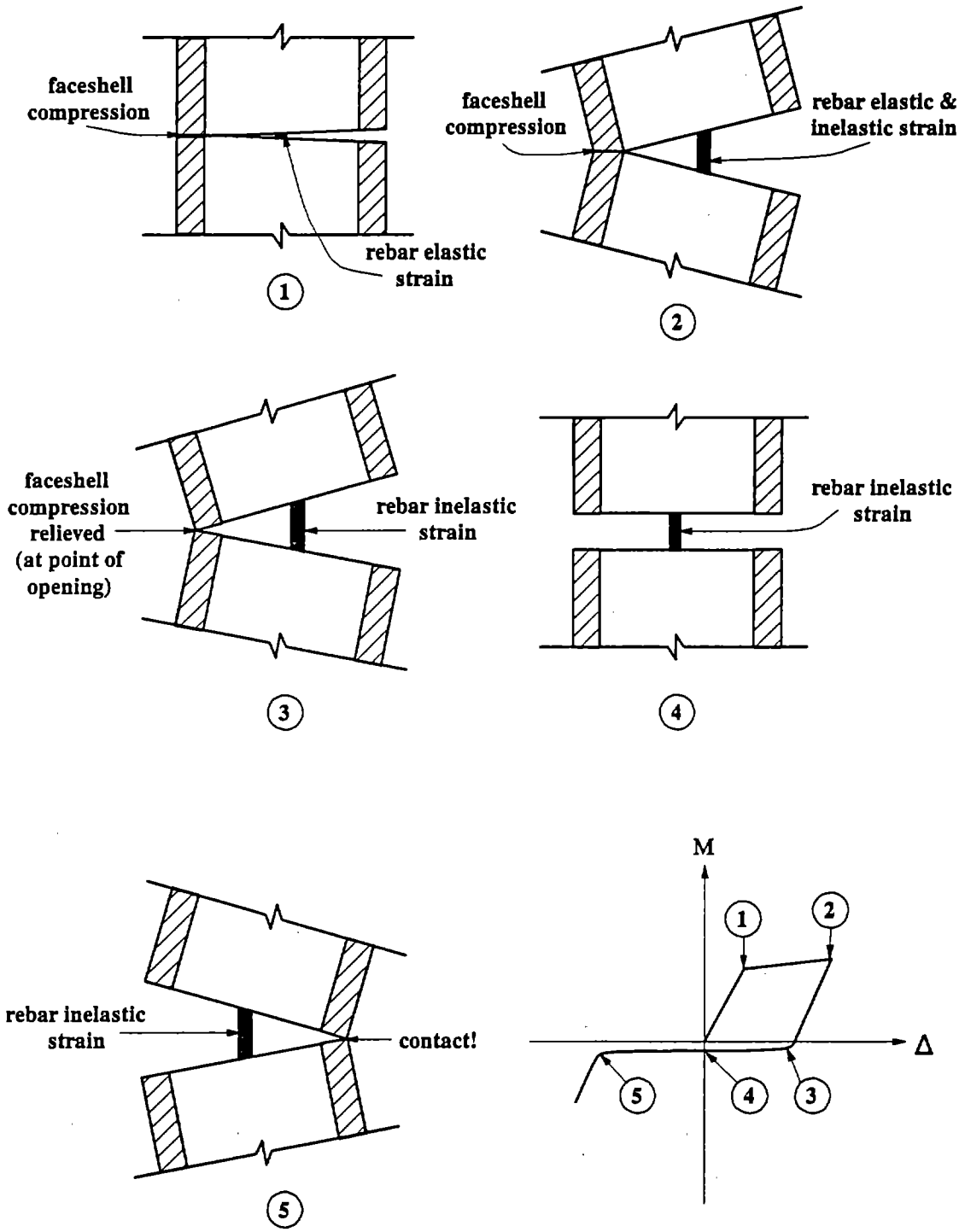

Figure 5: Post-Yield Cyclic Behavior

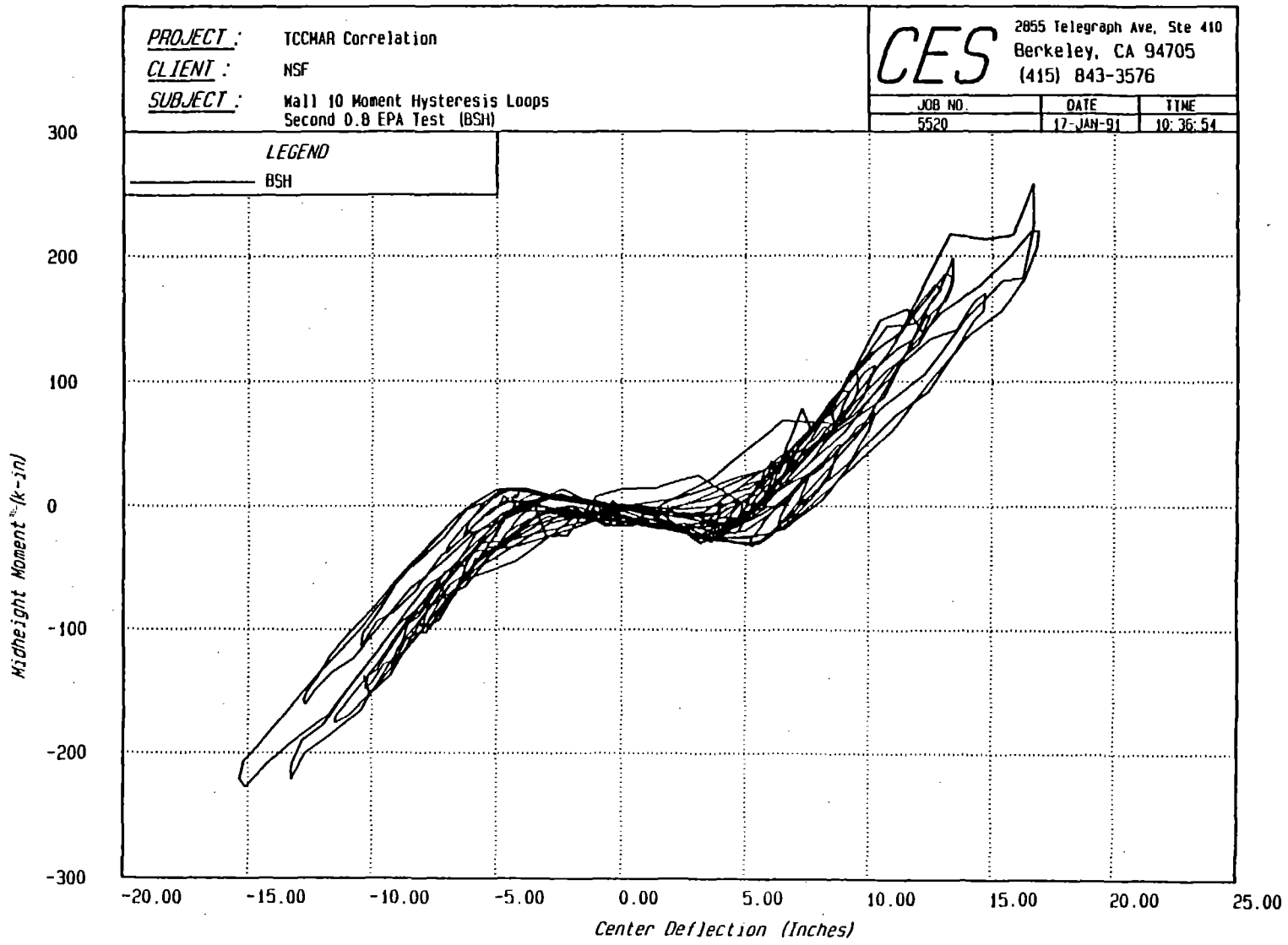

Figure 6: Wall 10 Post-Yield Moment Hysteresis Loops

Basic Model

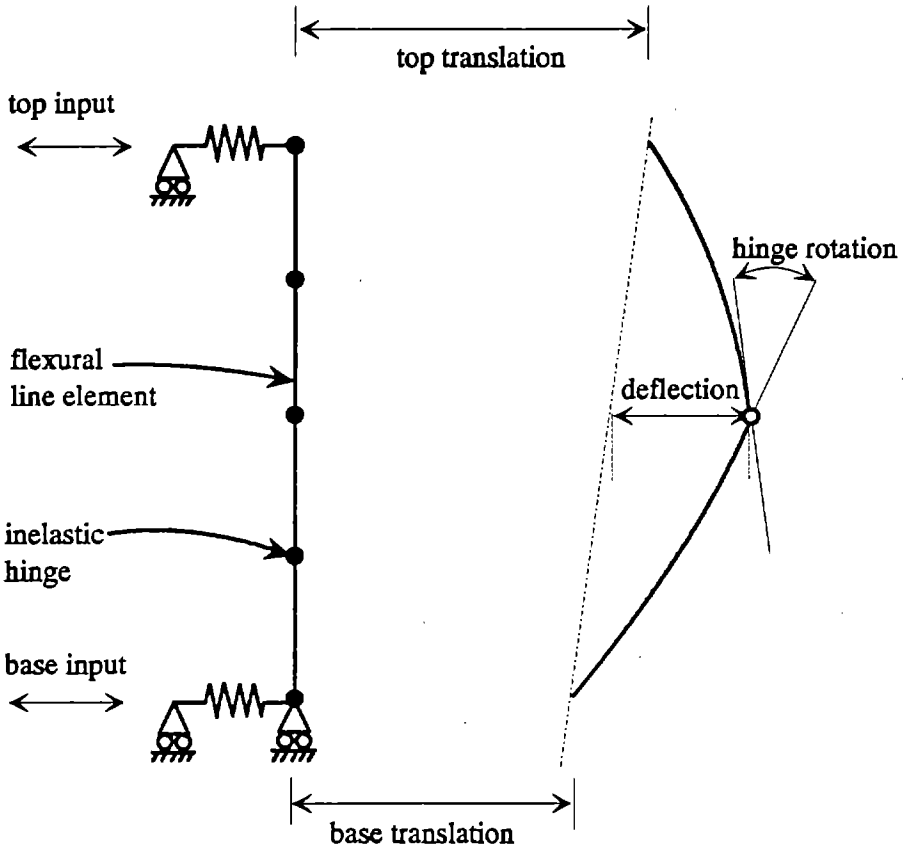

Figure 7: Analytical Model

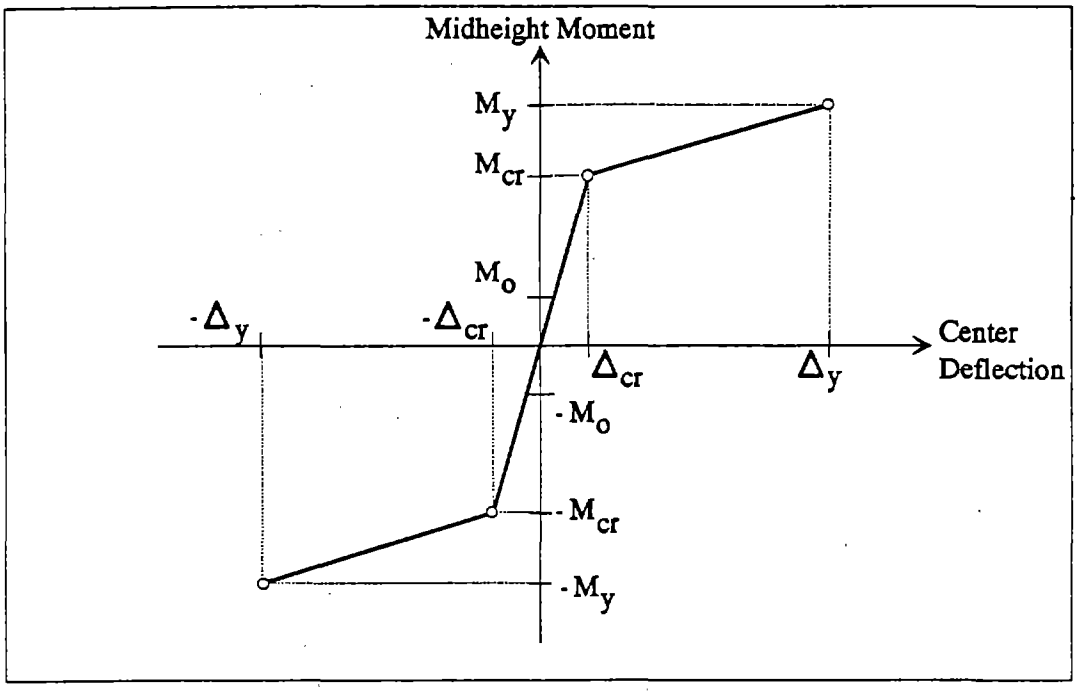

Figure 8: Moment Hysteresis Envelope or Virgin Curve

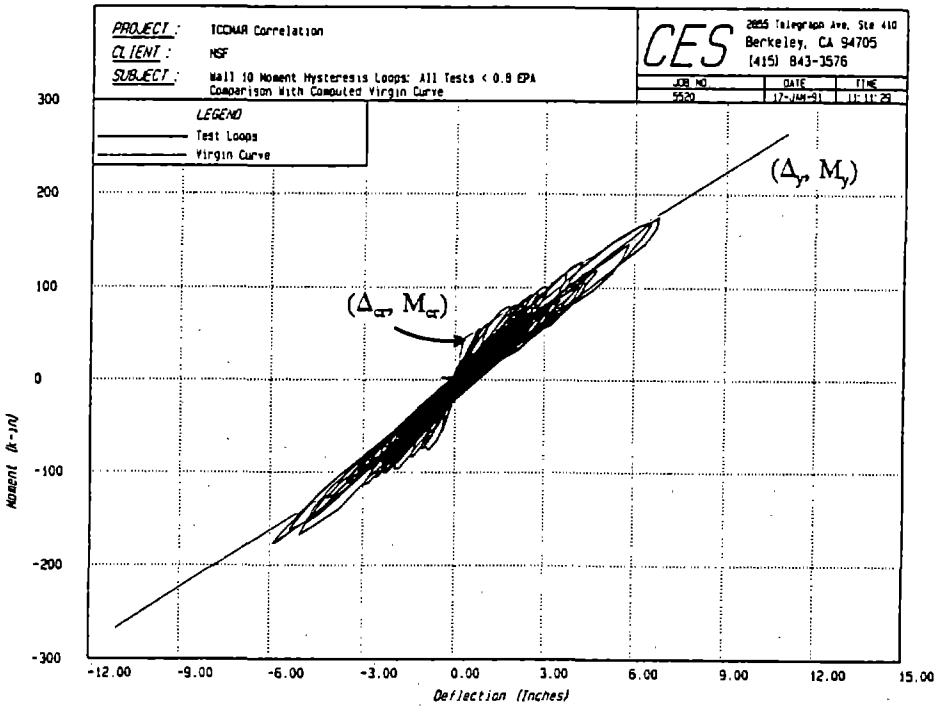

Figure 9: Computed Virgin Curve with Test Moment Hysteresis

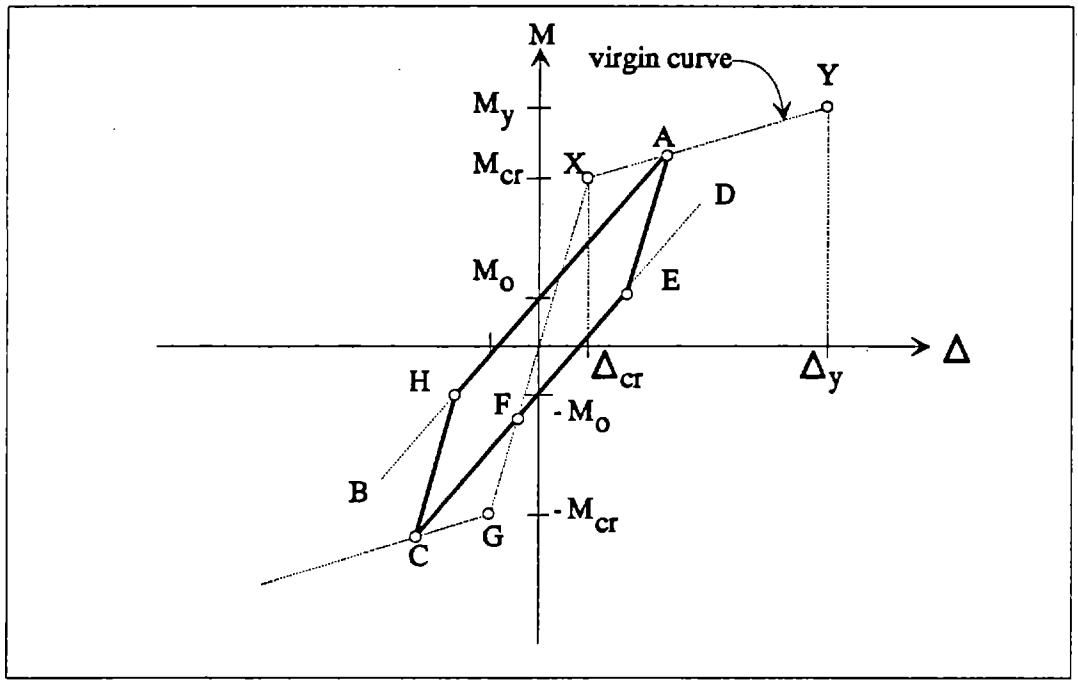

Figure 10: Analytical Hysteresis: Unloading After Cracking

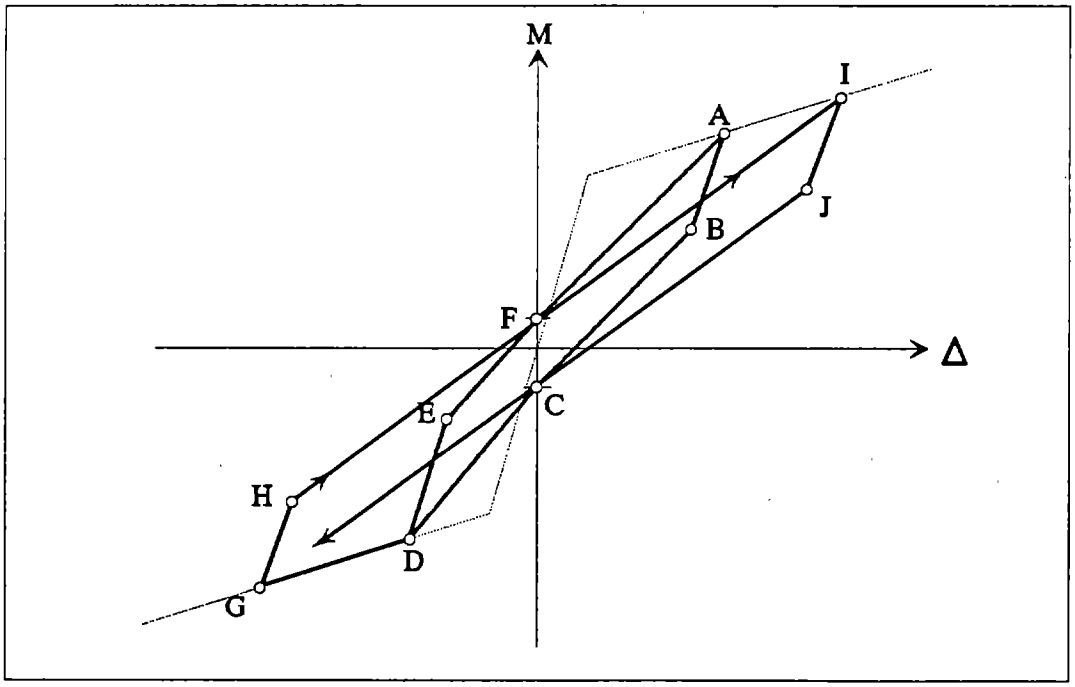

Figure 11: Analytical Hysteresis: Unequal Stiffness

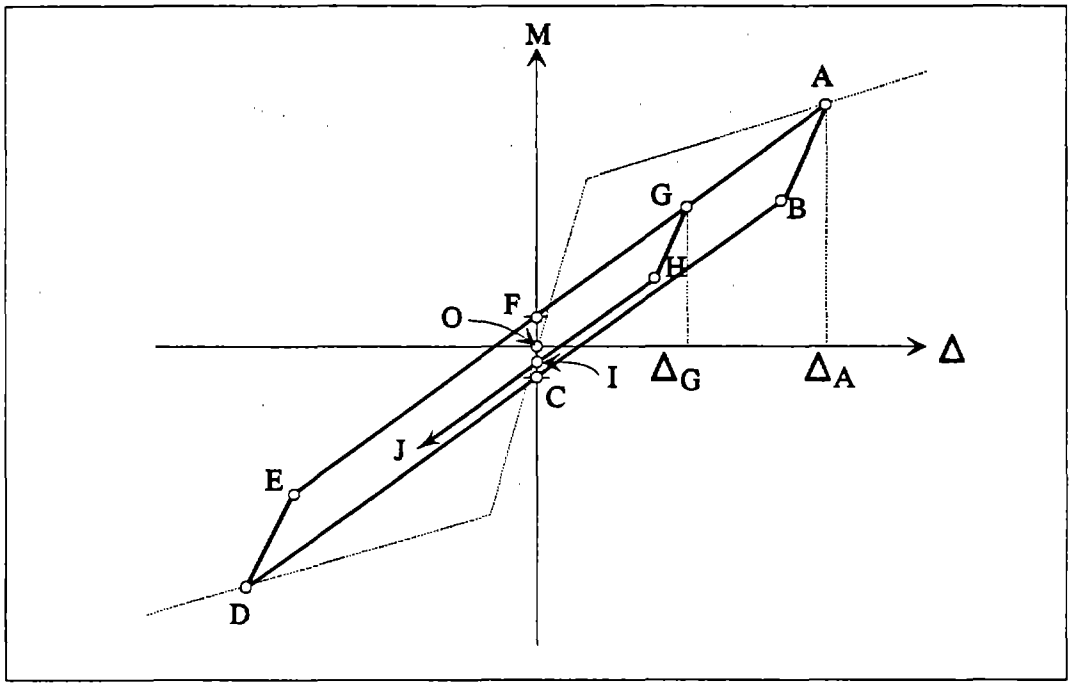

Figure 12: Analytical Hysteresis: Degrading Hysteresis Width

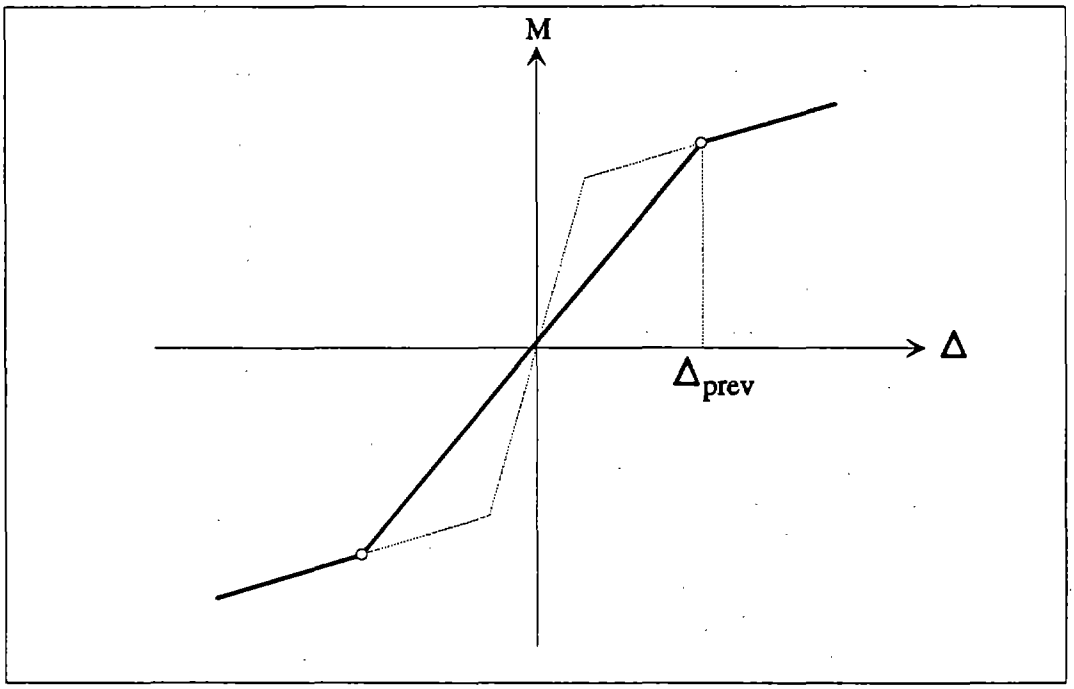

Figure 13: Analytical Hysteresis: Previous Maximum Deflection

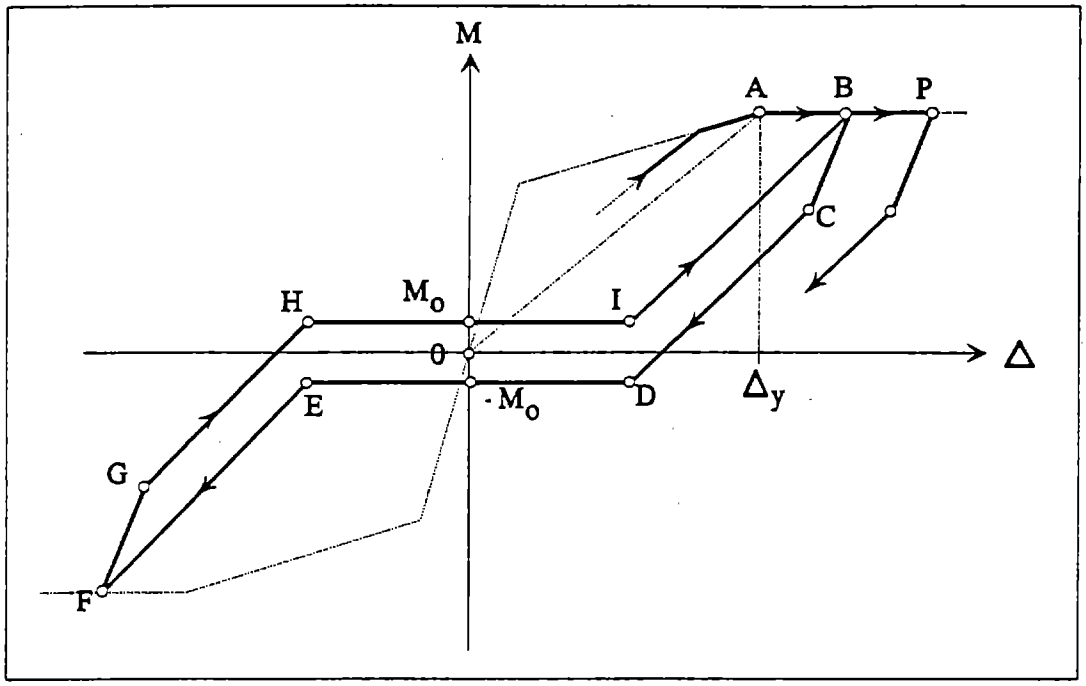

Figure 14: Analytical Hysteresis: Post-Yield Behavior

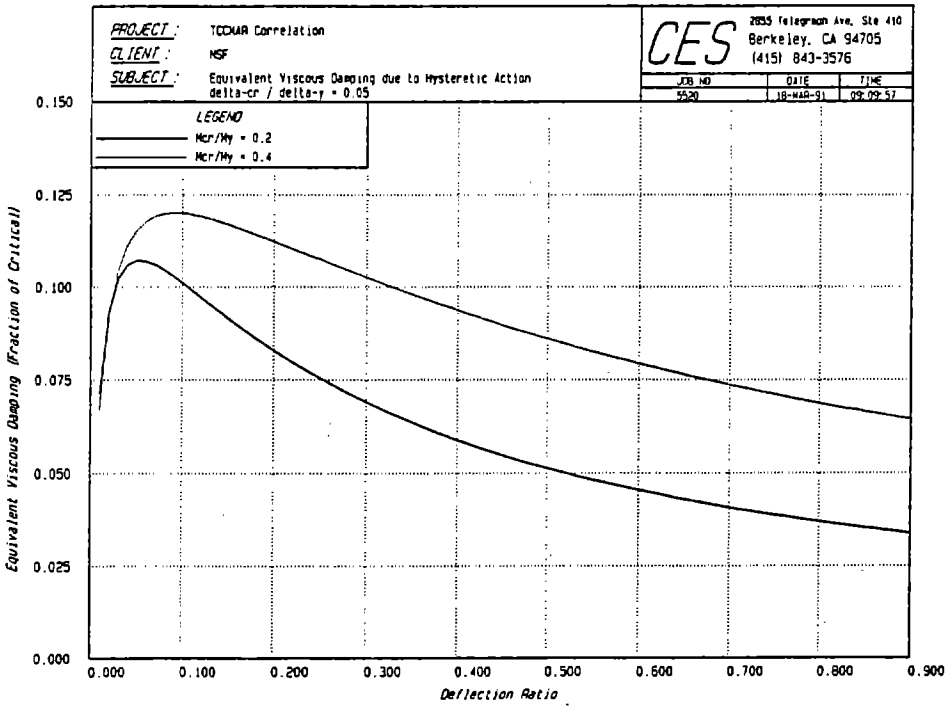

Figure 15: Equivalent Viscous Damping due to Hysteretic Action

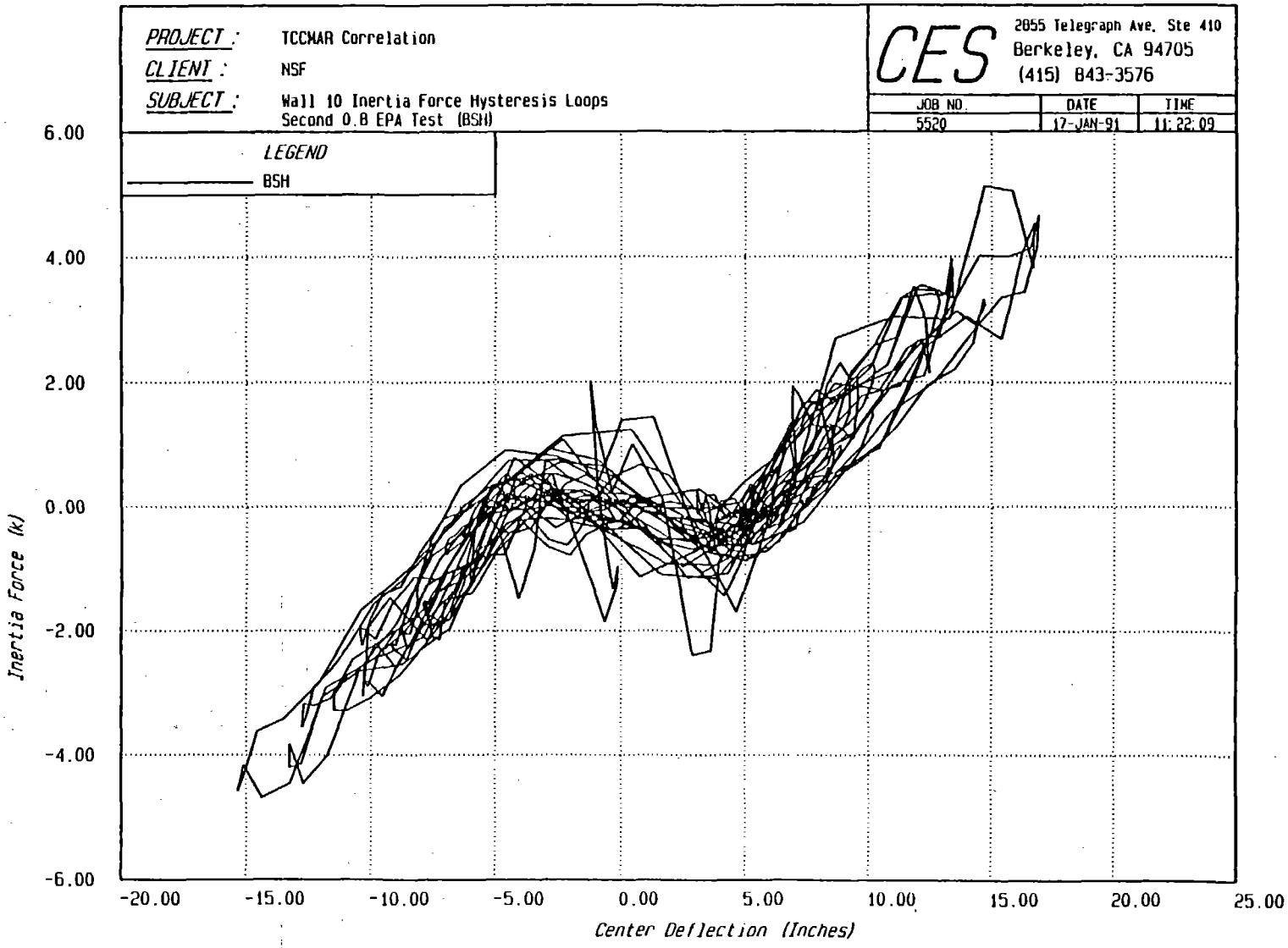

Figure 16: Wall 10 Inertia Force Hysteresis Loops for 0.8 EPA Test

4 Correlation of Analytical and Test Results

This section discusses the correlation between measured wall response during testing and analytical computation of that response. We begin with the clay brick walls, and a brief description of the correlation obtained with the first "static" tests on wall 1, then move to a more detailed presentation of correlation results for the dynamic tests on walls 9 and 10. Key results for the remaining five distinct clay brick walls (walls 3, 4, 6, 7 and 11) are then summarized. Finally, we discuss the correlation obtained for selected tests on concrete block walls.

The following notation is used to describe the set of 12 input motions during the dynamic tests on the clay brick walls:

MS1 - 0.1 EPA Hollister-Glorietta warehouse, Morgan Hill 1984
MS2 - 0.1 EPA Saratoga Valley College Gym, Morgan Hill 1984
TF1 - 0.1 EPA Lincoln School Tunnel, Taft 1952
EC1 - 0.1 EPA El Centro 1940
TF2 - 0.2 EPA Lincoln School Tunnel, Taft 1952
EC2 - 0.2 EPA El Centro 1940
BDC - 0.4 EPA Bonds Corner 1979
EC4 - 0.4 EPA El Centro 1940
BCS - 0.4 EPA Bonds Corner 1979
TFS - 0.4 EPA Lincoln School Tunnel, Taft 1952
BCH - 0.8 EPA Bonds Corner 1979
BSH - 0.8 EPA Bonds Corner 1979

A more complete description of these motions, including scaling techniques and conditions assumed to arrive at the top support motions can be found in [2].

4.1 Static Tests on Clay Brick Wall 1

Wall 1 was tested under static cycling at increasing displacement amplitudes. The wall was restrained against displacement at its third points, and equal displacements were applied at the top and bottom. The wall was subjected to sufficiently large displacements to cause yielding of the vertical steel. A full description of the test procedures and results can be found in [9].

A six-element model of the wall was formulated, and static, cyclic displacements were applied. Inelastic action in the model was confined to the inelastic hinge at the midheight of the wall. The remainder of the model deformed elastically in flexure at the uncracked stiffness. This is in contrast to the distributed non-linearities over the entire central third of the test walls. The displacement patterns of the test and model walls are shown in Figure 17.

Applying the test support displacements directly to the model, and plotting the sum of the reactions at the third points against the relative central deflection for various amplitudes of cycling, leads to the plots shown in Figures 18 and 19. These plots show the stabilized analytical hysteresis loops as solid lines, with straight dashed lines connecting the peak points in the stabilized test hysteresis loops. On examining these plots, it appears that the force levels are represented well by the analysis, but that the model is too flexible.

However, it must be remembered that the displacement patterns between the test wall and the model are very different. Given these displacement patterns, the model is locked into producing a larger relative deflection for a given support displacement than the test wall with its distributed softening. In addition, the model is designed to accurately predict the dynamic central relative deflection — the hysteresis is based on this deflection, and it is recognized that model deflections at other locations in the wall height will be inaccurate. As far as dynamic behavior is concerned, the loading arrangement in the static tests is artificial — only the relative deflection is important. Therefore, to test the dynamic model fairly against the static tests, the test center relative deflections should be reproduced in the model. This implies running reduced support displacements to produce the test relative deflections in the model. When this is done, the plots in Figures 20 and 21 result. Each of these figures show two plots: one with the analytical loops as solid lines and the test maxima joined by dashed lines, the other a reproduction of the actual test hysteresis loops. These figures show good agreement between overall hysteretic behavior in the test wall and the analytical model.

An alternative approach is to take the model response at the full test displacements, and modify the displacement at the center of the model by "spreading" the concentrated non-linearity of the hinge over the central third of the wall in an effort to represent the distributed softening apparent in the test wall. This can be achieved by fitting a beam function (uniform EI) between the tangents to the model deflected shape at the third-points as indicated in Figure 17. This reduces the central absolute displacement of the model by a factor of approximately two, and the central relative deflection to about 5/6 of the model value. Thus, when the test support displacements are used on the dynamic model with the above correction to the central deflection, the plot in Figure 22 results. Here too, the analytical loops are shown as solid lines, while a straight dashed line joins the test maxima. Again, excellent agreement is indicated between analytical and test responses.

Thus the correlation with the static test results indicates that the model is capable of reproducing the overall behavior of out-of-plane walls up to and beyond yield. In addition, the destabilizing effects of vertical load are also captured well as indicated in the negative stiffness region of Figure 21.

4.2 Dynamic Tests on Clay Brick Wall 9

Wall 9 is a 25 foot high wall with 2 #5 vertical rebars providing a steel content of $0.16\rho_b$. Each rebar is spliced at two locations within the wall height. Wall 9 is partially grouted, and supports a ledger load of 300 lb/ft.

An analytical model of this wall was subjected to each of the test motions in turn. Estimates were made of the condition of the wall at the start of each dynamic run, and this condition was reflected in the previous maximum deflection specified for each simulation. Viscous damping was generally set at 1% of critical, except in cases at relatively high levels of shaking where the test deflection was significantly smaller than the deflection in previous runs (for example, the last two 0.4 EPA runs, where the previous maximum test deflection was 8.8" during run EC4, but the test maximum deflections in the subsequent two runs were 4.68" and 5.31" respectively). Under these conditions, the analytical model remains elastic at a stiffness based on the previous maximum deflection, and no hysteretic damping is apparent until that previous maximum deflection is exceeded. However, due to the presence of distributed cracked joints in the physical wall, the actual response demonstrates a significant hysteretic area.

The loss of hysteretic damping in the analytical model is accounted for with an increase in viscous damping, the magnitude of which can be gauged from Figure 15. This figure presents the equivalent viscous damping at full cycles as a function of wall deflection. The low amplitudes (compared to previous maxima) present in the response mean that there will be a degradation in hysteretic width relative to the width at the previous maximum, and a corresponding decrease in the equivalent viscous damping. At a deflection of 8.8 inches, the full equivalent viscous damping is about 7% for wall 9, and it is assumed that at reduced deflections about half of this amount will be present. Thus, in the analytical model, the viscous damping in these runs is increased from 1% to 5%.

An interesting observation arises in the case of the first dynamic test on wall 9. If the analysis assumes that the wall was initially uncracked, a maximum deflection of 0.36 inches is predicted. This is a mere 18% of the measured deflection of 1.98 inches. If the assumption is made that the wall had been previously cracked during handling, and (arbitrarily but reasonably) that the wall had experienced a deflection of 1 inch prior to the start of the first test, then the analysis predicts a deflection of 2.34 inches. Thus tremendous sensitivity to the initial state of the wall is apparent.

Table 4.1 summarizes the experimental and analytical results for wall 9. Three measures of wall response are recorded. These are the maximum center relative deflections, the maximum midheight moments in the wall, and the maximum of the sum of top and bottom reactions in the wall. The experimental reactions are the inertia forces computed from measured accelerations corrected for the effects of the vertical load and the self weight of the wall. Data in this table is presented graphically in Figures 23, 24 and 25.

Agreement between analysis and experiment in terms of the maximum responses is generally very good for deflections, moments and reactions. It should be noted that the analytical modelling of the second 0.8g run (BSH) is imprecise. That test starts with a wall that has already experienced yielding. The capability to represent that situation is currently unavailable in the analytical model. Thus, the analytical results presented are for a wall which starts the test just below yield. This gives a reasonable estimate of the actual response of the wall.

Run ID	EPA (g)	Deflection (in)		Moment (k-in)		Reaction (k)	
		Test	Analysis	Test	Analysis	Test	Analysis
MS1	0.1	1.98	2.34	59.5	59.9	1.13	0.96
MS2	0.1	0.49	0.43	23.3	24.7	0.38	0.32
TF1	0.1	1.10	0.95	36.2	50.0	0.62	0.74
EC1	0.1	1.65	2.12	47.1	57.1	0.86	0.97
TF2	0.2	3.13	2.57	69.7	61.1	1.07	0.89
EC2	0.2	2.14	2.04	59.8	58.0	0.91	0.84
BDC	0.4	5.77	5.87	84.7	83.9	1.30	1.25
EC4	0.4	8.80	7.32	107.7	93.6	1.75	1.18
BCS	0.4	4.68	5.11	58.4	60.0	0.80	0.74
TFS	0.4	5.31	6.15	64.9	71.7	0.98	1.13
BCH	0.8	11.17	12.81	112.1	108.5	1.84	1.35
BSH	0.8	16.79	16.08	109.2	108.7	1.47	1.48

Table 4.1 : Correlation Results for Wall 9

When test and analysis maxima are averaged over each EPA level, the ratios of analytical response to test response are shown in Table 4.2.

EPA (g)	Analysis / Test		
	Deflection	Moment	Reaction
0.1	1.11	1.15	1.00
0.2	0.87	0.92	0.87
0.4	1.00	0.98	0.89
0.8	1.03	0.98	0.86

Table 4.2 : Response Ratios for Wall 9

This table indicates that the analytical model provides excellent estimates of deflection and moment over all EPA levels. Reactions are predicted adequately, with averages typically 10% to 15% low at the higher EPA levels.

In addition to good prediction of test maxima, the details of the response are also well represented by the analytical model. Typical comparative plots of center deflection time history are shown in Figures 26 (run TF1, 0.1 EPA), 27 (run BDC, 0.4 EPA) and 28 (run BCH, 0.8 EPA). The frequency content, maxima and trace form from the tests are all well captured in the analytical results. Typical comparative plots of moment hysteresis loops from test and analysis are presented in Figures 29 (run TF2, 0.2 EPA), 30 (run BDC, 0.4 EPA) and 31 (run BCH, 0.8 EPA). Note that in each of these plots, the test hysteresis loops have been offset from the analytical ones for the sake of clarity. This offset is 2" in the case of Figure 29, 4" for Figure 30 and 10" for Figure 31. The analytical loops agree well with those measured during the test program.

Based on the results presented in this section, it is clear that the analytical model performs well in predicting the response of wall 9 during the dynamic tests.

4.3 Dynamic Tests on Clay Brick Wall 10

Wall 10 is a 25 foot high wall with 3 #7 vertical rebars providing a steel content of $0.50\rho_b$. Each rebar is spliced at two locations within the wall height. Wall 10 is partially grouted, and supports a ledger load of 300 lb/ft.

An analytical model of this wall was subjected to each of the test motions in turn. Estimates were made of the condition of the wall at the start of each dynamic run, and this condition was reflected in the previous maximum deflection specified for each simulation. Viscous damping was generally set at 1% of critical, except in cases where the test deflection was significantly smaller than the previous maximum deflection (runs TF1, EC2, BCS and TFS: for example, the last two 0.4 EPA runs, where the previous maximum test deflection was 6.78" during run EC4, but the test maximum deflections for BCS was 4.36" and that for TFS was 4.41"). Under these conditions, the analytical model remains elastic at a stiffness based on the previous maximum deflection, and no hysteretic damping is apparent until that previous maximum deflection is exceeded. However, due to the presence of distributed cracked joints in the physical wall, the actual response demonstrates a significant hysteretic area.

The loss of hysteretic damping in the analytical model is accounted for with an increase in viscous damping, the magnitude of which can be gauged from Figure 15. This figure presents the equivalent viscous damping at full cycles as a function of wall deflection. The low amplitudes (compared to previous maxima) present in the response mean that there will be a degradation in hysteretic width relative to the width at the previous maximum, and a corresponding decrease in the equivalent viscous damping. At a deflection of 6.78 inches, the full equivalent viscous damping is about 5% for wall 10, and it is assumed that at reduced deflections about half of this amount will be present. Thus, in the analytical model, the viscous damping in these runs is increased from 1% to 4%.

Table 4.3 summarizes the experimental and analytical results for wall 10. Three measures of wall response are recorded. As for wall 9, these are the maximum center relative deflections, the maximum midheight moments in the wall, and the maximum of the sum of

top and bottom reactions in the wall. The experimental reactions are the inertia forces computed from measured accelerations corrected for the effects of the vertical load and the self weight of the wall. The data in this table is presented graphically in Figures 32, 33 and 34.

Agreement between analysis and experiment in terms of the maximum response is generally very good for deflections, moments and reactions. It should be noted that the analytical modelling of the second 0.8g run (BSH) is imprecise. That test starts with a wall that has already experienced yielding. The capability to model that situation is currently unavailable in the analytical model. Thus, the analytical results presented are for a wall which starts the test just below yield. This gives a reasonable estimate of the actual response of the wall.

Run ID	EPA (g)	Deflection (in)		Moment (k-in)		Reaction (k)	
		Test	Analysis	Test	Analysis	Test	Analysis
MS1	0.1	0.47	0.37	53.8	58.9	1.18	1.06
MS2	0.1	0.72	0.68	67.3	53.5	1.17	1.12
TF1	0.1	0.26	0.40	25.6	35.2	0.53	0.64
EC1	0.1	1.02	1.06	76.2	61.4	1.35	1.28
TF2	0.2	3.09	2.67	103.5	95.6	2.04	1.66
EC2	0.2	2.06	2.14	67.7	72.8	1.13	1.19
BDC	0.4	6.52	6.83	169.9	180.7	3.12	2.97
EC4	0.4	6.78	8.10	176.8	201.3	3.32	3.32
BCS	0.4	4.36	4.03	109.7	104.2	2.03	1.73
TFS	0.4	4.41	4.38	128.1	118.3	2.23	1.99
BCH	0.8	15.71	15.07	285.0	267.3	5.01	4.29
BSH	0.8	16.93	16.10	260.5	267.4	4.21	4.27

Table 4.3 : Correlation Results for Wall 10

When test and analysis maxima are averaged over each EPA level, the ratios of analytical response to test response are shown in Table 4.4.

EPA (g)	Analysis / Test		
	Deflection	Moment	Reaction
0.1	1.02	0.94	0.97
0.2	0.94	0.98	0.90
0.4	1.06	1.02	0.93
0.8	0.96	0.98	0.93

Table 4.4 : Response Ratios for Wall 10

This table indicates that the analytical model generally predicts deflections and moments within 5% of the corresponding measured values for all EPA levels. In addition, the average reactions for all EPA levels are within 10% of the corresponding average test values.

In addition to good prediction of test maxima, the details of the response are also well represented by the analytical model. Typical comparative plots of center deflection time history are shown in Figures 35 (run MS2, 0.1 EPA), 36 (run EC2, 0.2 EPA), 37 (run BDC, 0.4 EPA) and 38 (run BCH, 0.8 EPA). The frequency content, maxima and trace form from the tests are all very well captured in the analytical results. Typical comparative plots of moment hysteresis loops from test and analysis are presented in Figures 39 (run MS2, 0.1 EPA), 40 (run EC2, 0.2 EPA), 41 (run BDC, 0.4 EPA) and 42 and 43 (run BCH, 0.8 EPA). Note that in each of these plots, the test hysteresis loops have been offset from the analytical ones for the sake of clarity. This offset is 0.25" in the case of Figure 39, 2" for Figure 40, 4" for Figure 41 and 10" for Figure 42. Figure 43 presents the same data as Figure 42, except here the analytical and test loops are superimposed without offset to emphasize the excellent correlation attained by the analytical model. We also note the lack of hysteretic area in the model for run EC2 which causes a lower level of response than the previous 0.2 EPA run (run TF2). The test hysteretic area is modelled in this case by increased viscous damping as explained previously. The analytical loops all correlate well with those measured during the test program.

Based on the results presented in this section, it is clear that the analytical model performs very well in predicting the response of wall 10 during the dynamic tests.

4.4 Dynamic Tests on Remaining Clay Brick Walls

Summary tables corresponding to Tables 4.2 (wall 9) and 4.4 (wall 10) are presented here for the remainder of the dynamic walls. The results reported in this section use 1% viscous damping, except in cases where hysteretic damping is absent in the model. This occurs when a run induces significantly lower response than some previous run on that wall, as explained in Sections 4.2 and 4.3. In these cases, additional viscous damping is supplied to account for

the hysteretic damping present in the test wall. The amount of additional damping is chosen with reference to Figure 15, using the procedure described previously.

One consistent source of potential difference between analytical and experimental responses for the walls in this section is that the input motions to the analytical models were those recorded during the tests on wall 10, rather than those actually recorded on the corresponding wall. While good control of the input signals was maintained during the test program, it is inevitable that some differences existed between the "same" signals on two different walls, which would mean minor differences in the responses. Based on Figure 8 in reference [5], it appears that this source of error in the analytical modelling has a maximum effect of about 10%.

Walls 3 and 5 are 25 feet in height with 3 #7 vertical rebars. There are no splices in the rebars, and the both walls are fully grouted. The ledger load is 800 lb/ft. Table 4.5 summarizes the correlation obtained for these walls. The measured responses of walls 3 and 5 were very similar as indicated in [5]. The test results used here are for wall 3.

EPA (g)	Analysis / Test		
	Deflection	Moment	Reaction
0.1	1.33	1.04	0.93
0.2	2.51	1.19	0.85
0.4	1.12	1.20	0.90
0.8	1.15	0.96	0.98

Table 4.5 : Response Ratios for Wall 3

Table 4.5 demonstrates that the model does a good job of predicting the observed responses, except for the deflections at the 0.2 EPA level, where the model overestimates the response by a factor of 2. The observed deflections in walls 3 and 5 at the 0.2 EPA level are significantly lower than for the remaining 25 foot walls. This phenomenon appears to be linked to the larger ledger load on walls 3 and 5.

Wall 4 is 20 feet in height with 2 #5 vertical rebars and no splices. It is fully grouted and supports a ledger load of 50 lb/ft except for the 0.8g runs when the ledger load was increased to 300 lb/ft. Table 4.6 summarizes the correlation obtained for this wall.

EPA (g)	Analysis / Test		
	Deflection	Moment	Reaction
0.1	0.85	0.95	0.97
0.2	0.86	0.85	0.88
0.4	0.85	0.94	0.98
0.8	0.91	0.81	1.08

Table 4.6 : Response Ratios for Wall 4

The analytical modelling of wall 4 produces responses which are in good agreement with those observed during the testing for all EPA levels.

It should be pointed out here that for wall 4, the standard set of 12 runs was augmented with 6 additional runs (two at 0.2g, three at 0.4g and one at 0.5g). In addition, the standard order of the 0.4g tests was changed for wall 4, with EC4 occurring before BDC. This difference in order of testing highlights the sensitivity of wall response to the initial condition of the wall. Table 4.7 shows the center maximum deflection for these two 0.4g runs. The test results are shown, together with the analytical results for the actual test order, then the analytical results for the standard test order (the difference being the previous maximum deflection). The match with observed deflections is much superior when the actual test order is used in analysis, dramatically demonstrating the influence of the initial stiffness of the wall on its out-of-plane seismic response.

Run	Test Deflection (in)	Analytical Deflection (in)	
		Test Order	Standard Order
EC4	4.49	4.03	7.12
BDC	7.77	5.72	2.24

Table 4.7 : Effect of Run Order for Wall 4

There was general yielding in wall 4 during test run BDC at the 0.4 EPA level. As explained previously, the analytical model is currently unable to start in a post-yielded state, so in analytical runs after BDC, the model was started with an initial stiffness based on a previous deflection just below yield. Since an actual yielded wall starts a subsequent test with essentially no stiffness, this modelling is approximate at best, and clearly influences the

response the model in the 0.4g and 0.8g runs. However, the general trends observed in the testing of wall 4 are reflected well in the analytical results.

Wall 6 is also 20 feet in height with 2 #5 vertical rebars and no splices. It is fully grouted and supports a ledger load of 300 lb/ft. Table 4.8 summarizes the correlation obtained for this wall.

EPA (g)	Analysis / Test		
	Deflection	Moment	Reaction
0.1	0.90	0.90	0.78
0.2	0.90	1.01	1.01
0.4	1.09	0.96	0.91
0.8	1.15	0.83	1.01

Table 4.8 : Response Ratios for Wall 6

The analytical modelling of wall 6 produces responses which are in good agreement with those observed during the testing for all EPA levels.

As for wall 4, the standard set of 12 runs was augmented with 6 additional runs (two at 0.2g, three at 0.4g and one at 0.5g). In addition, the standard order of the 0.4g tests was changed for wall 6, and these tests occurred as EC4, BDC, TFS and BCS. This difference in order of testing highlights the sensitivity of wall response to the initial condition of the wall. Table 4.9 shows the center maximum deflection for the first two 0.4g runs (EC4 and BDC). The test results are shown, together with the analytical results for the actual test order, then the analytical results for the standard test order (the difference being the previous maximum deflection). As for wall 4, the match with observed deflections is much superior when the actual test order is used in analysis, again demonstrating the strong influence of the initial stiffness of the wall on its out-of-plane seismic response.

Run	Test Deflection (in)	Analytical Deflection (in)	
		Test Order	Standard Order
EC4	2.07	2.09	3.53
BDC	2.58	2.68	2.09

Table 4.9 : Effect of Run Order for Wall 6

There was general yielding in wall 6 during the 0.5g non-standard test. As explained previously, the analytical model is currently unable to start in a post-yielded state, so in the analytical runs at the 0.8g level, the model was started with an initial stiffness based on a previous deflection just below yield. Since an actual yielded wall starts a subsequent test with essentially no stiffness, this modelling is approximate at best, and clearly influences the response the model during the 0.8g runs. However, the general trends observed in the testing of wall 6 are reflected well in the analytical results.

Wall 7 is 25 feet in height with 3 #7 vertical rebars and no splices. It is fully grouted and supports a ledger load of 300 lb/ft. Table 4.10 summarizes the correlation obtained for this wall.

EPA (g)	Analysis / Test		
	Deflection	Moment	Reaction
0.1	0.87	0.95	0.91
0.2	1.08	0.93	0.87
0.4	0.95	0.82	0.70
0.8	0.94	0.97	0.91

Table 4.10 : Response Ratios for Wall 7

Table 4.10 demonstrates that the model predicts the response of wall 7 with reasonable accuracy. Deflections are slightly underestimated at the 0.1g level, but are predicted well at the remaining EPA levels. Moments are predicted reasonably well except at the 0.4g level where they are underestimated by about 20%. Reactions are underestimated by about 10% at all levels except the 0.4g level where they are underestimated by about 30%.

Wall 11 is also 25 feet in height with 3 #7 vertical rebars and no splices. It is partially grouted (cells containing rebars only) and supports a ledger load of 300 lb/ft. Table 4.11 summarizes the correlation obtained for this wall.

The first thing to note from Table 4.11 is that there are two entries for the 0.1 EPA level. The very first run (MS1) on wall 11 produces a center deflection of 2.14". If the analysis assumes that the wall starts test MS1 uncracked, then the analytical deflection for run MS1 is only 0.37" or 17% of the test deflection. The first line in Table 4.11 (marked 0.1 U for "uncracked") gives the results based on an initially virgin wall. Wall 10 (similar to wall 11 except for spliced rebars) has an experimental deflection of 0.47" under run MS1. It appears that the lack of splices in wall 11 are insufficient to account for the 0.47" to 2.14" difference in deflection, which leads to the conclusion that wall 11 was somehow damaged in handling prior to the start of the test sequence. If it is assumed that the wall has been previously cracked, with the (arbitrary but reasonable) assumption that the wall had previously seen a deflection of 1", then the analytical deflection under run MS1 is 1.72" or 80% of the test

deflection. The second line in Table 4.11 (marked 0.1 C for "cracked") gives the results based on an initially cracked wall, and confirms the hypothesis that the wall was initially cracked.

EPA (g)	Analysis / Test		
	Deflection	Moment	Reaction
0.1 U	0.64	0.86	0.81
0.1 C	0.90	0.97	0.92
0.2	1.08	0.96	0.92
0.4	1.01	0.82	0.71
0.8	1.04	0.82	0.70

Table 4.11 : Response Ratios for Wall 11

The rest of Table 4.11 demonstrates that the model predicts the deflection response of wall 11 with reasonable accuracy. Deflections are well predicted at all levels, while at the 0.4g and 0.8g levels, moments are generally underestimated by about 20% and reactions by about 30%.

4.5 Dynamic Tests on Concrete Block Walls

Correlation with the dynamic tests on concrete block walls (Task 3.2(b1) of TCCMAR) was also performed. In these tests [3], four walls each 20 feet in height were tested under a wide variety of seismic conditions in a similar set-up to that described previously for the clay brick walls. Correlation between analytical and test center relative deflection is presented here for two of the walls, referred to as walls 2 and 3 in [3].

Wall 2 is 20 feet in height, 39.5" in width and 4.5" thick, giving an H/t ratio of 53. The wall is reinforced vertically with two #4 reinforcing bars for a steel content of about 25% of the balanced reinforcement. There are no splices in the vertical steel, and the wall is fully grouted. The wall carries a static vertical ledger load of 300 lb/ft, and is pin-supported at both top and base, and is excited by a pair of hydraulic actuators, one at the base, the other at the top of the wall. The results for run 6 (Castaic, 1971, N69W, scaled to be consistent with a 0.4g S1 spectrum, stiff top diaphragm) are used here for the purpose of correlation.

Wall 3 is also 20 feet in height and 39.5" in width, but this wall uses 5.625" blocks, giving an H/t ratio of 43. The wall is reinforced vertically with two #5 reinforcing bars for a steel content of about 31% of the balanced reinforcement. There are no splices in the vertical steel, and the wall is partially grouted. The wall carries a static vertical ledger load of 300

lb/ft, and is pin-supported at both top and base, and is excited by a pair of hydraulic actuators, one at the base, the other at the top of the wall. The results for runs 5 (El Centro, 1940, S00E, scaled to be consistent with a 0.4g S1 spectrum, flexible top diaphragm), 9 (El Centro, 1940, S00E, scaled to be consistent with a 0.4g S1 spectrum, stiff top diaphragm, compressed time scale) and 26 (Bonds Corner, 1979, scaled in the frequency domain to be consistent with a 0.8g S1 spectrum, flexible top diaphragm) are used here for the purpose of correlation.

The test report [3] states that the actual motions imparted to the test walls contained less energy than the target motions. The report further states that

> " ... the existing experimental data can still be used for future analytical and/or numerical model calibration since the actual input motion imparted on the specimens are known."

It is the measured test motions which are used here as input to the analytical model for correlation purposes.

Table 4.12 presents the peak midheight deflection for each of the above runs from both test measurements and analytical predictions. The analytical maxima agree very well with the observed test maxima in all cases. Figures 44 to 47 present the traces of center deflection for both test and analysis for each of the cases in Table 4.12. These figures clearly demonstrate that not only the maxima, but also the analytical frequency content is in excellent agreement with the test results.

No correlations are presented here for moment or reaction, since, unfortunately, these quantities were neither measured directly nor deduced from measurements made during the concrete block wall test program.

Wall	Run	Test (in)	Analysis (in)	Analysis / Test
2	6	2.07	2.22	1.07
3	5	1.19	1.03	0.87
3	9	2.81	3.52	1.25
3	26	3.62	3.60	0.99

Table 4.12 : Midheight Deflection for Walls 2 and 3

Based on these results, it is clear that the analytical model performs well in predicting the response of reinforced concrete block walls.

4.6 Summary

This section has presented the results of a detailed correlation study using the analytical model described in Section 3 of this report, and the results from tests on eleven full-scale reinforced clay brick walls. The tests on two walls were conducted at very slow rates and constitute the "static" tests. The remaining nine walls were each subjected to at least twelve dynamic motions representative of the various seismic zones in the United States. Several key parameters were varied over the nine dynamic walls, including H/t ratio, vertical reinforcement, grouting, splices and vertical ledger load. In addition, correlation runs were made for selected tests on two full-scale reinforced concrete block walls.

In all cases, the responses computed from the analytical model have been in good agreement with those observed during the test programs, over the full range of wall parameters for all intensities of seismic motion. Table 4.13 tabulates the distribution of the response ratios (analytical response / test response) for all the clay brick dynamic walls. There are seven distinct walls with four different EPA levels for each wall, giving a total of 28 response ratios for each of deflection, moment and reaction. The data in Table 4.13 is presented graphically in Figure 48, as three histograms.

Range of Response Ratio	Number of Occurrences		
	Deflection	Moment	Reaction
1.15 and above	4	3	0
1.05 to 1.14	6	0	1
0.95 to 1.04	7	14	7
0.85 to 0.94	11	6	16
0.75 to 0.84	0	5	1
Less than 0.75	0	0	3

Table 4.13 : Distribution of Response Ratios for All Clay Brick Walls

The statistics computed from the individual response ratios are presented in Table 4.14. The mean response ratios for deflection and moment are very close to 1.0, while for reactions, the mean ratio is 0.9. For each response quantity, the coefficient of variation (standard deviation divided by mean) is about 10%. This indicates that all key responses are predicted well by the analytical model. An alternative evaluation of the correlation is to examine the percentage of response ratios falling below 0.85 (a 15% underestimation of response). When this is done, none of the deflection response ratios are less than 0.85, 18% of the moment response ratios are less than 0.85 and 14% of the reaction response ratios fall below 0.85.

Response	Response Ratio Statistics	
	Mean	Standard Deviation
Deflection	1.00	0.12
Moment	0.96	0.10
Reaction	0.90	0.09

Table 4.14 : Response Ratio Statistics for Clay Brick Walls

A less detailed evaluation of the correlation obtained for the concrete block tests is possible, due to the lack of information recorded during those tests. Only deflection correlations were obtained, as only deflections were available from the test programs. The four tests used here for correlation purposes resulted in a mean deflection response ratio of 1.05.

Based on the results presented in this section, the analytical model performs well for a wide variety of wall types and excitation levels, and can be used with confidence to predict the out-of-plane response of reinforced masonry walls.

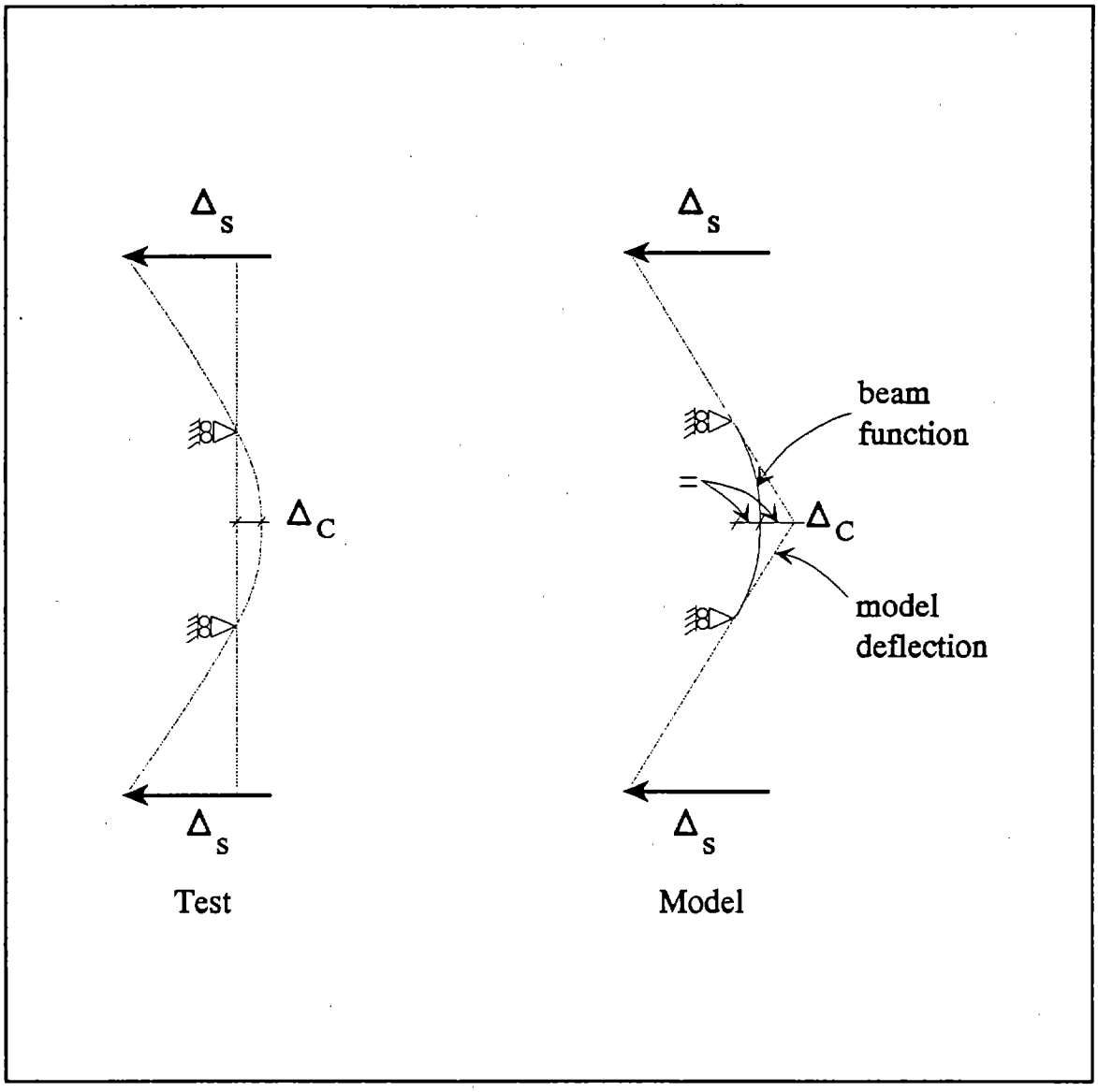

Figure 17: Displacement Patterns in Test and Model Walls

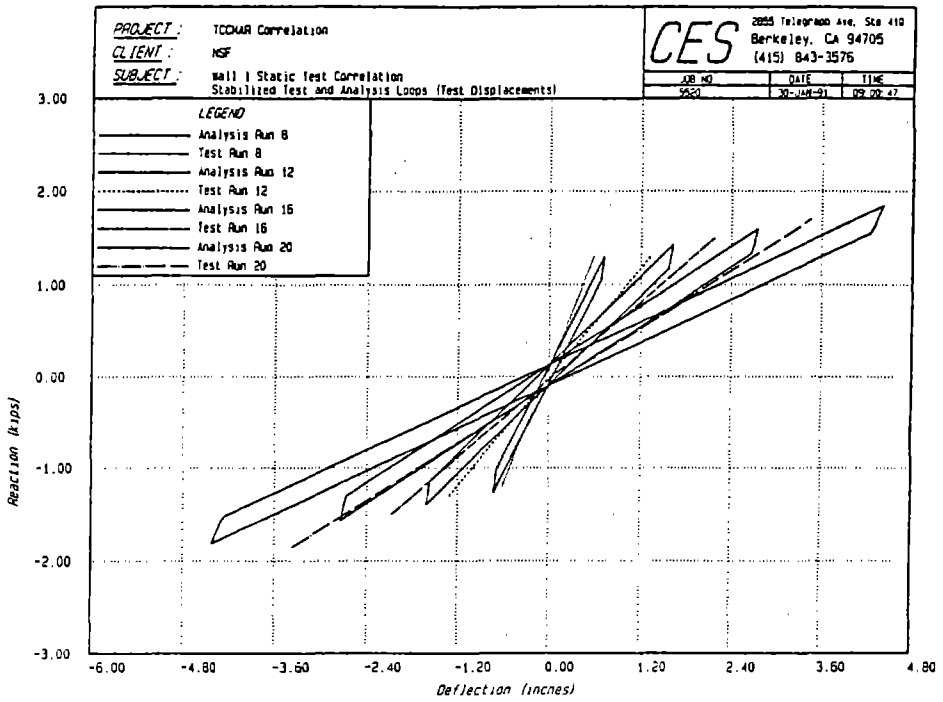

Figure 18: Wall 1 Pre-Yield Correlation: Test Displacements

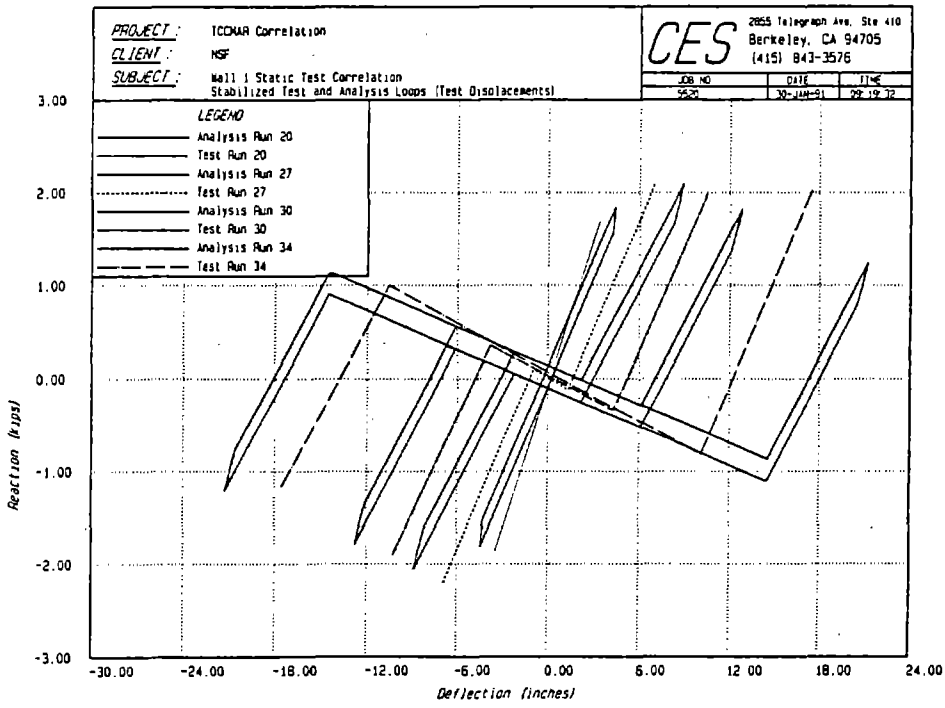

Figure 19: Wall 1 Post-Yield Correlation: Test Displacements

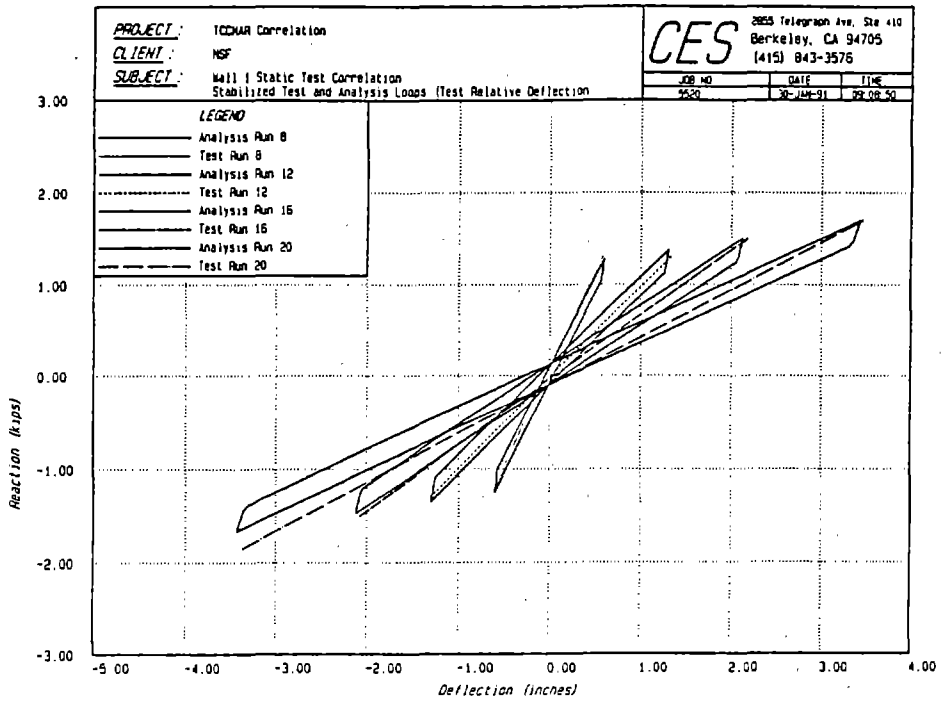

(a) Analysis with Test Maxima Joined by a Straight Line

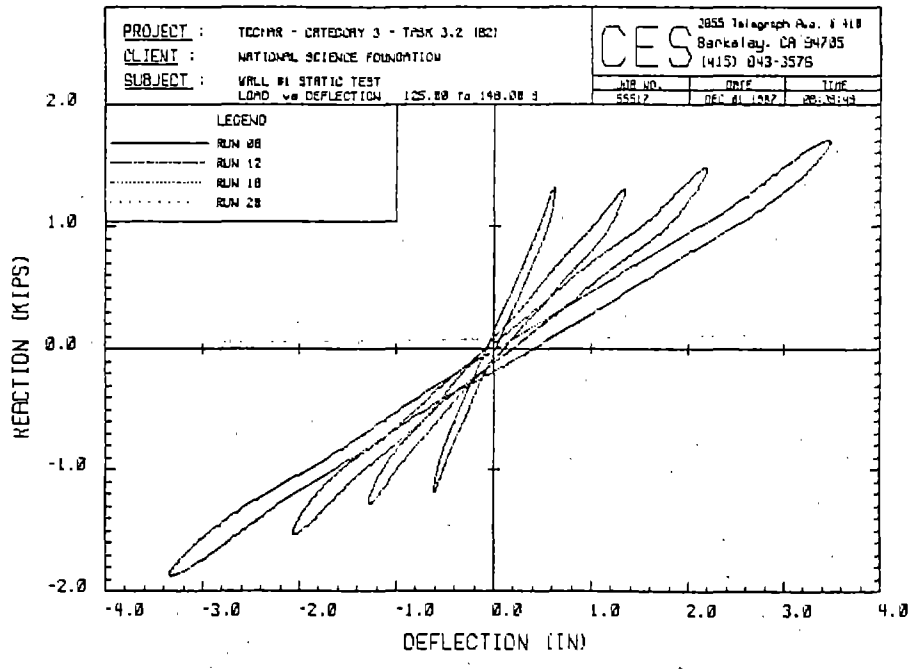

(b) Stabilized Test Hysteresis Loops

Figure 20: Wall 1 Pre-Yield Correlation: Test Relative Deflections

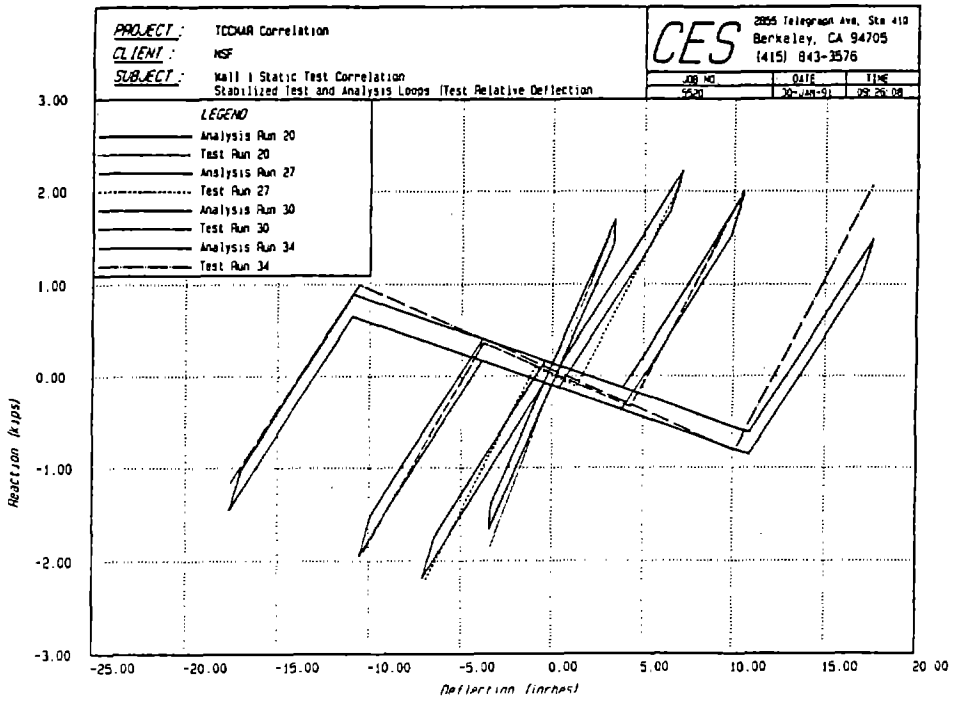

(a) Analysis with Test Maxima Joined by a Straight Line

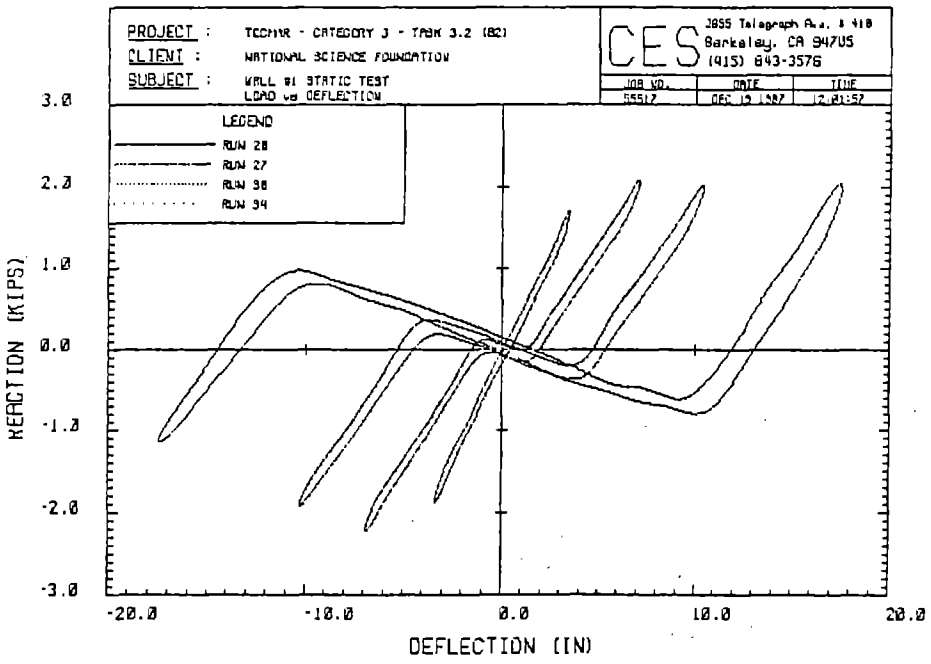

(b) Stabilized Test Hysteresis Loops

Figure 21: Wall 1 Post-Yield Correlation: Test Relative Deflections

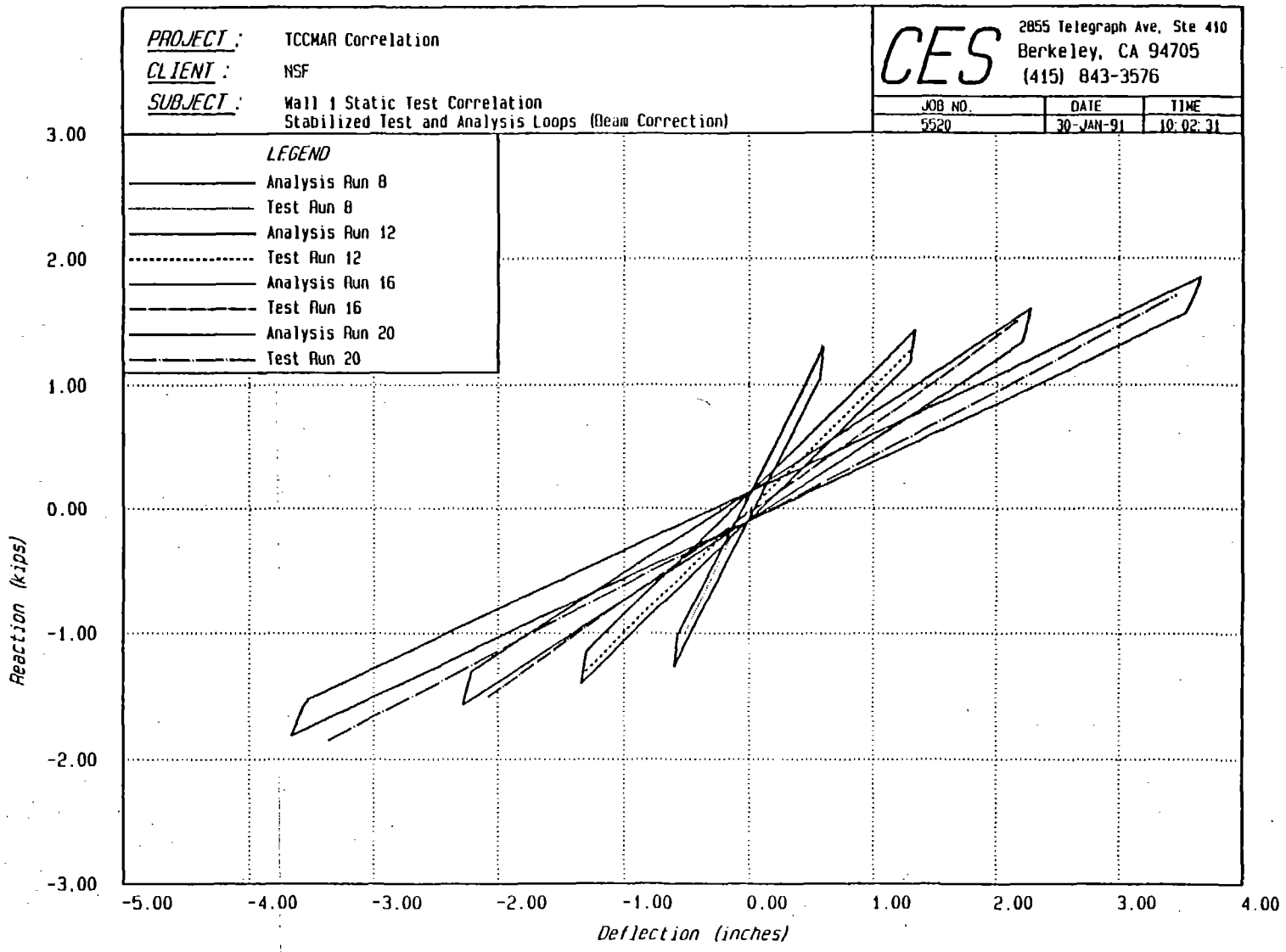

Figure 22: Wall 1 Pre-Yield Correlation: Beam Correction to Test Displacements

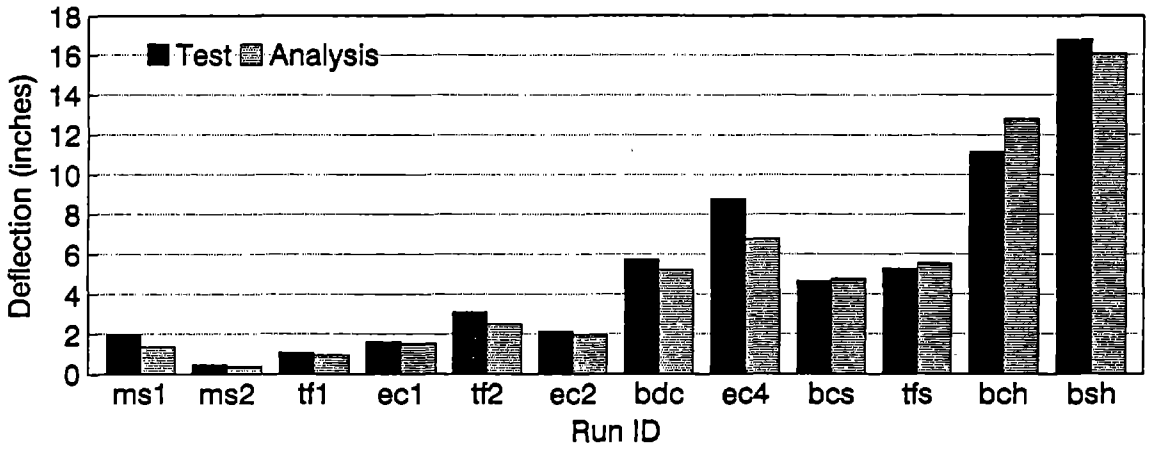

Figure 23: Comparison of Test and Analytical Deflections - Wall 9

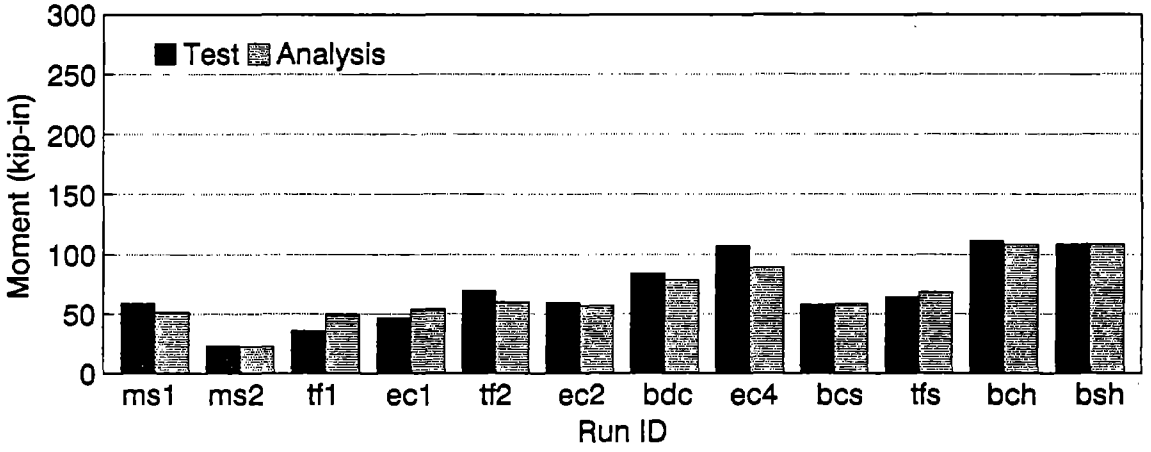

Figure 24: Comparison of Test and Analytical Moments - Wall 9

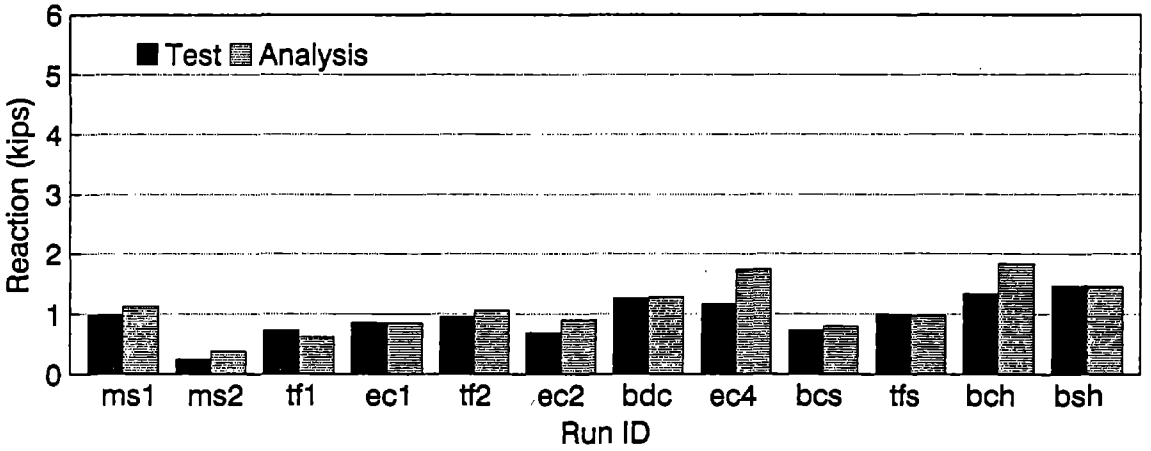

Figure 25: Comparison of Test and Analytical Reactions - Wall 9

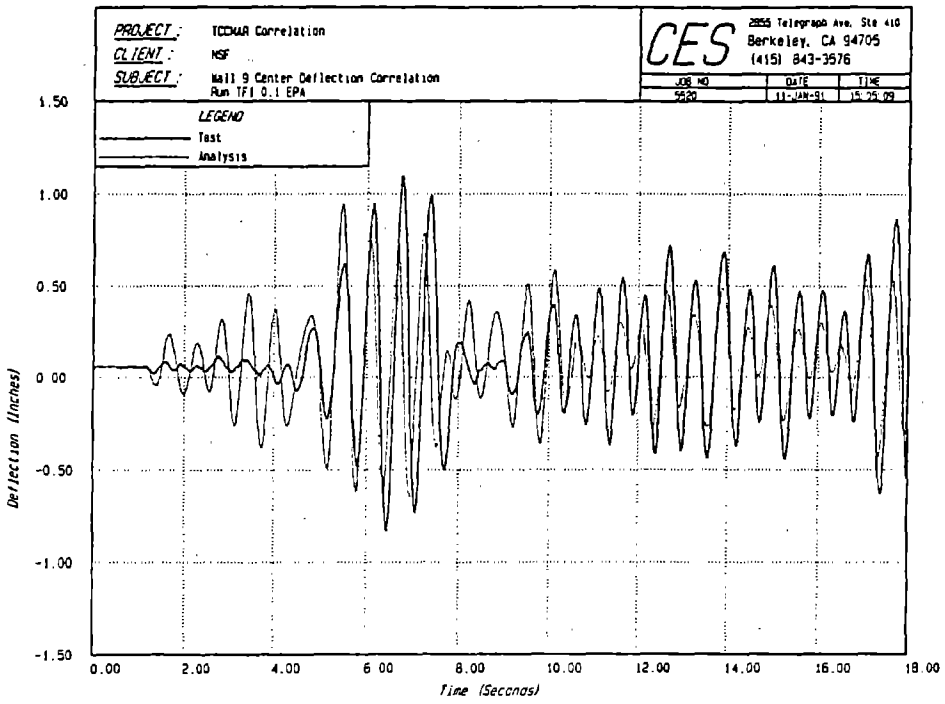

Figure 26: Comparison of Test and Analytical Deflections - Wall 9 Run TF1

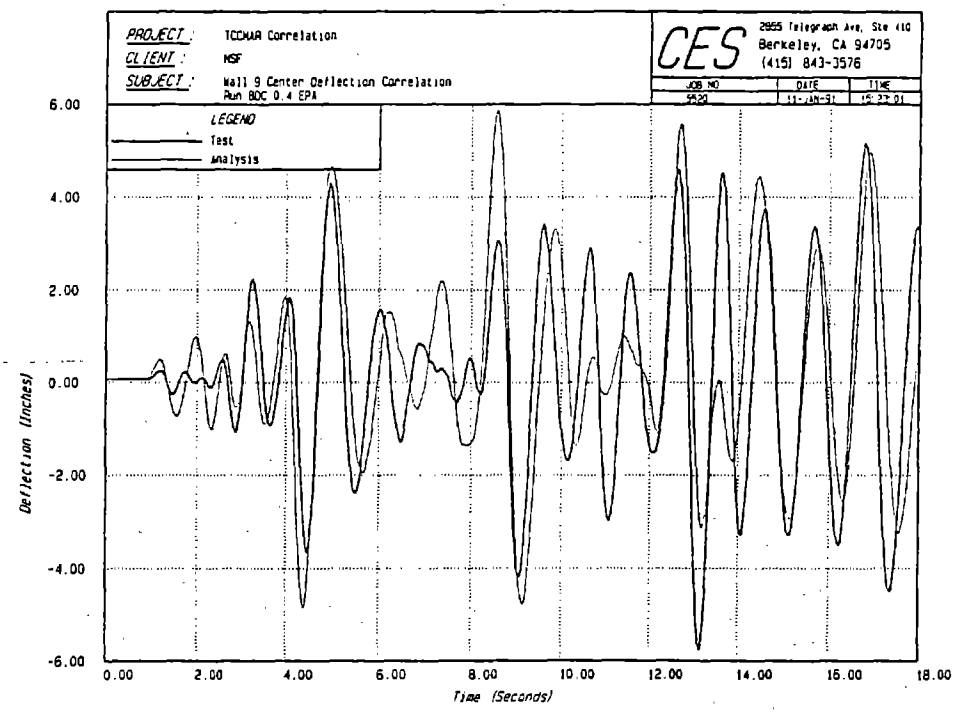

Figure 27: Comparison of Test and Analytical Deflections - Wall 9 Run BDC

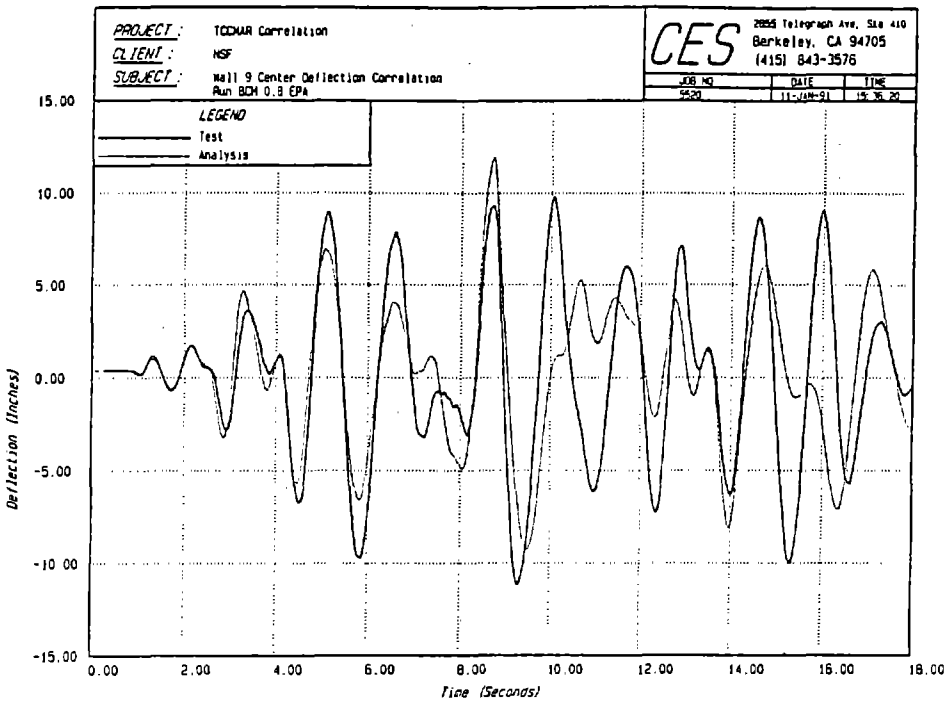

Figure 28: Comparison of Test and Analytical Deflections - Wall 9 Run BCH

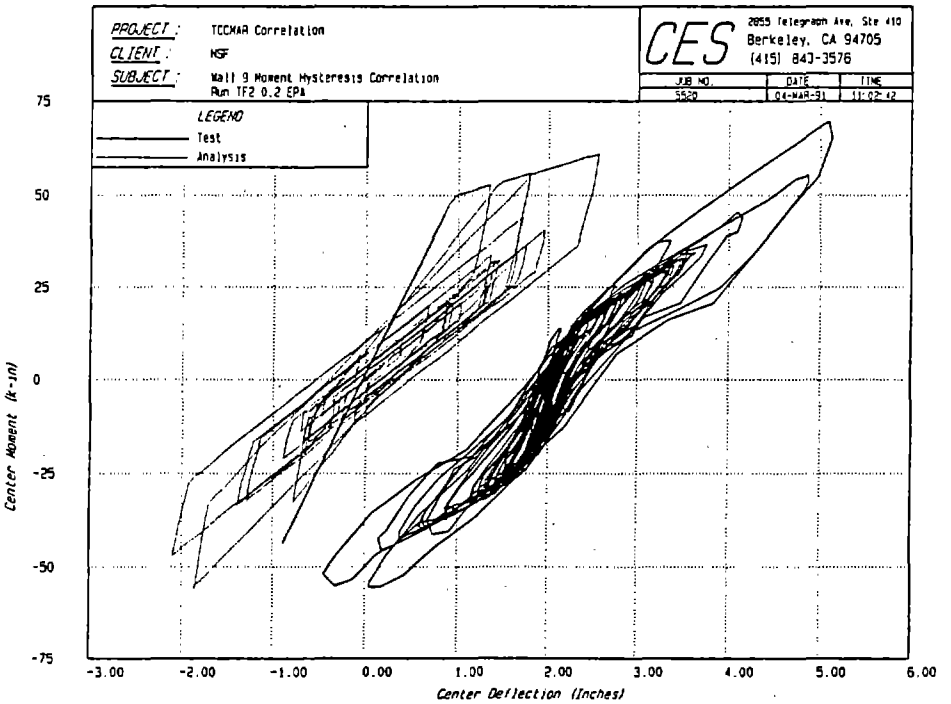

Figure 29: Comparison of Test and Analytical Hysteresis Loops - Wall 9 Run TF2 (Offset = 2")

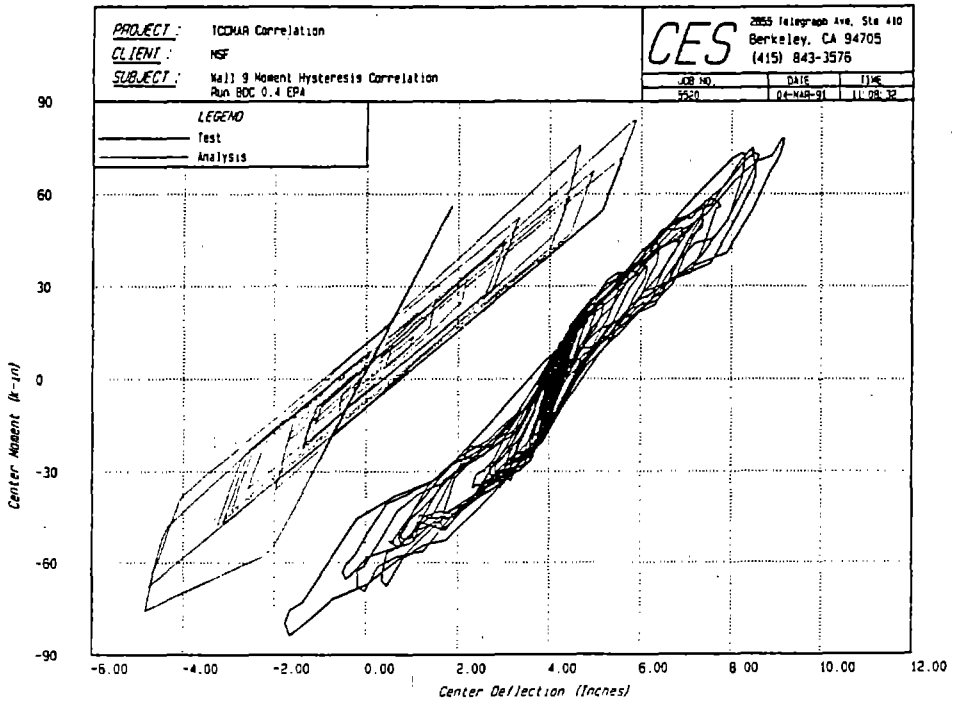

Figure 30: Comparison of Test and Analytical Hysteresis Loops - Wall 9 Run BDC (Offset = 4")

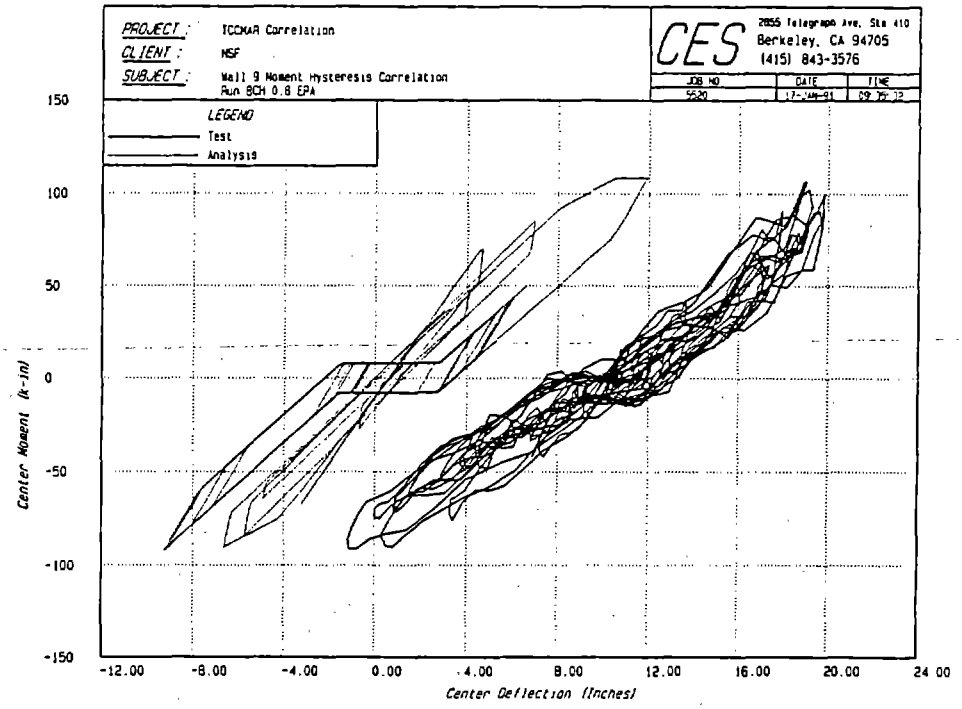

Figure 31: Comparison of Test and Analytical Hysteresis Loops - Wall 9 Run BCH (Offset = 10")

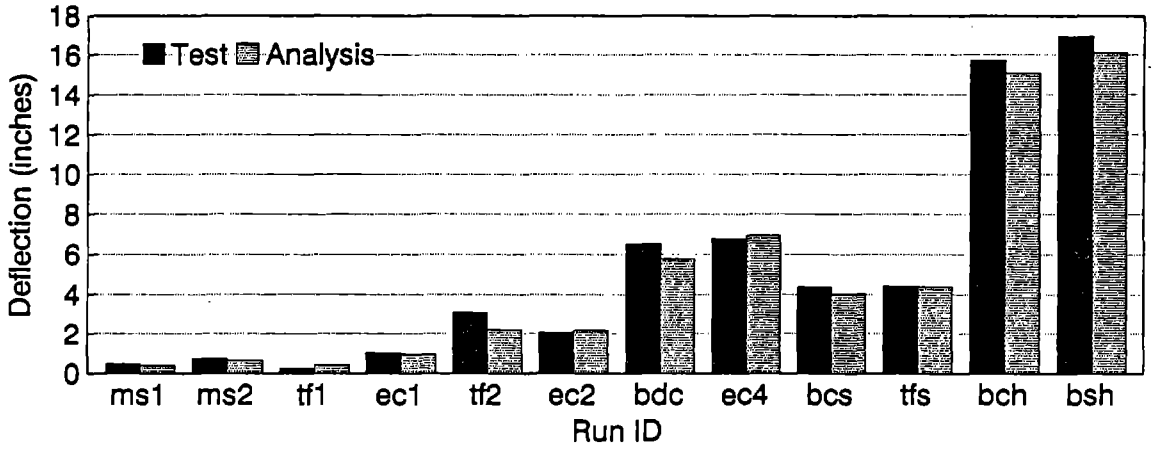

Figure 32: Comparison of Test and Analytical Deflections - Wall 10

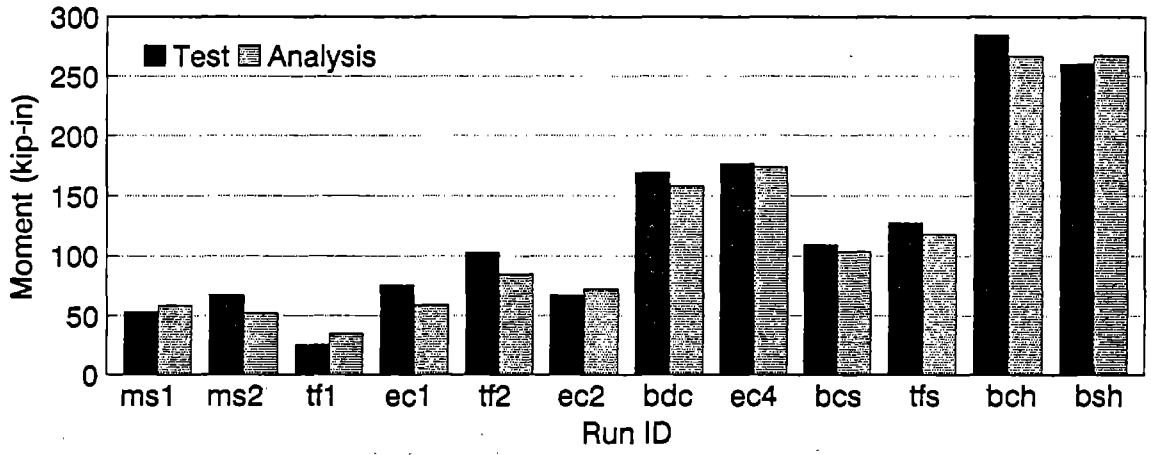

Figure 33: Comparison of Test and Analytical Moments - Wall 10

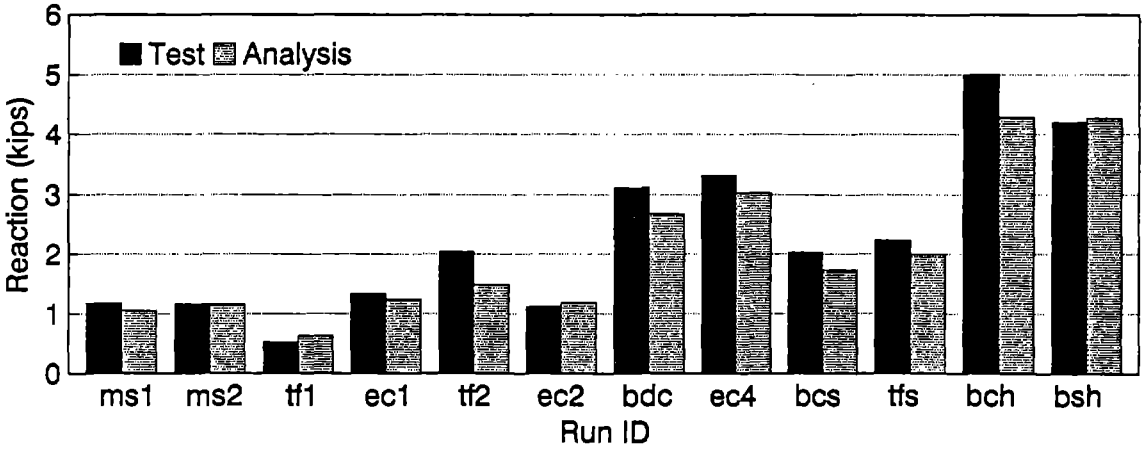

Figure 34: Comparison of Test and Analytical Reactions - Wall 10

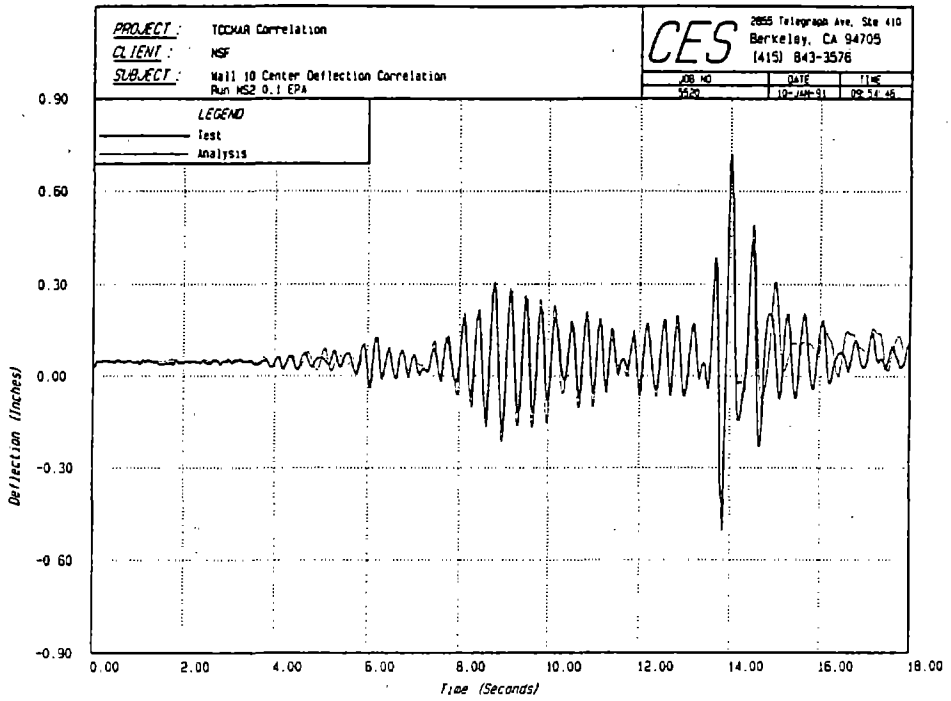

Figure 35: Comparison of Test and Analytical Deflections - Wall 10 Run MS2

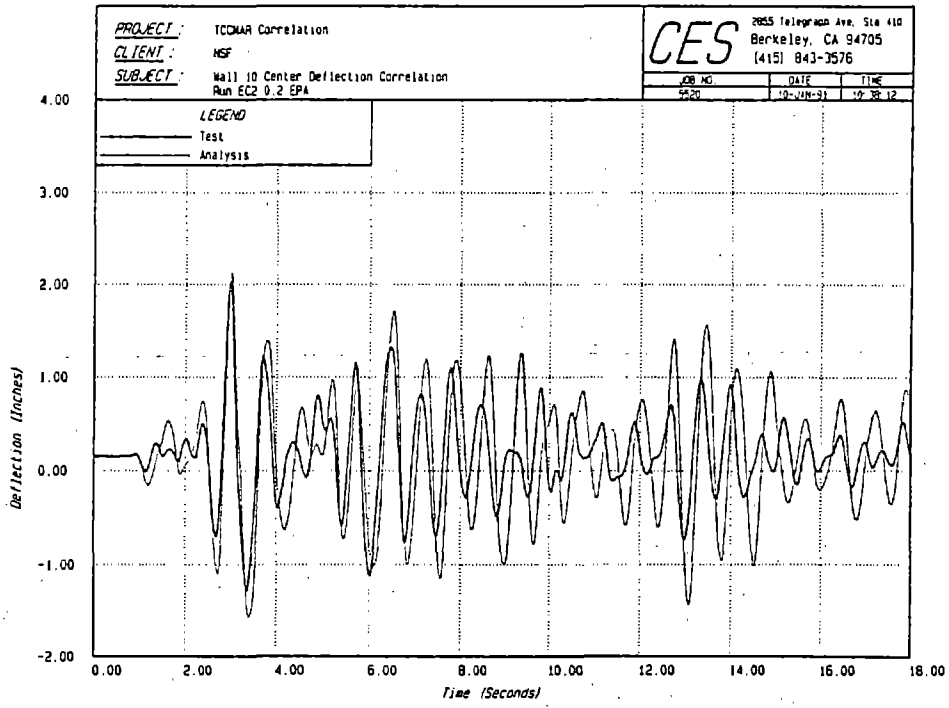

Figure 36: Comparison of Test and Analytical Deflections - Wall 10 Run EC2

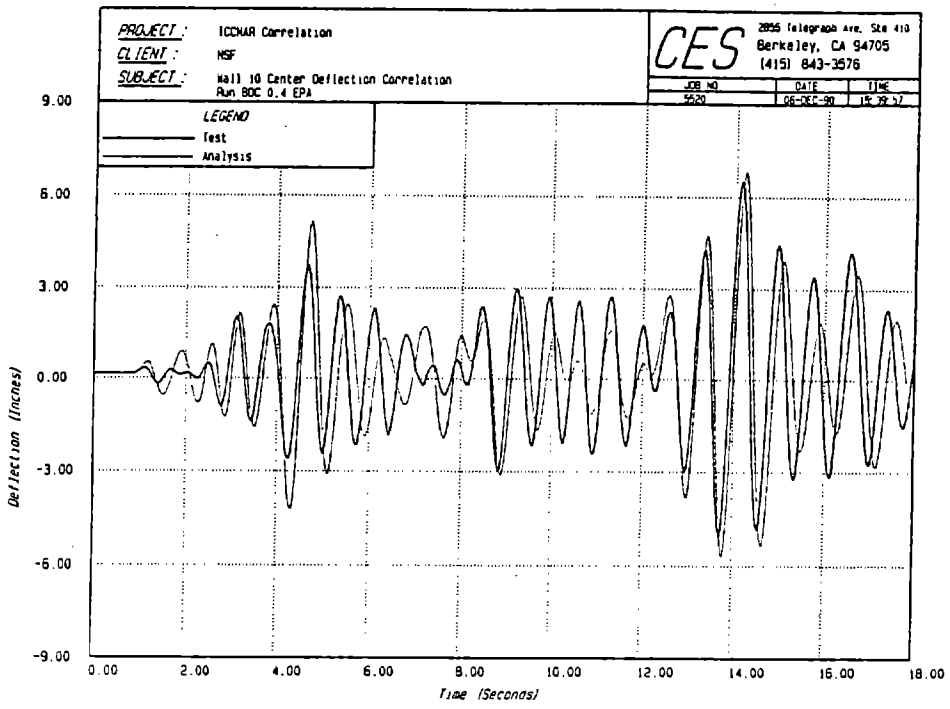

Figure 37: Comparison of Test and Analytical Deflections - Wall 10 Run BDC

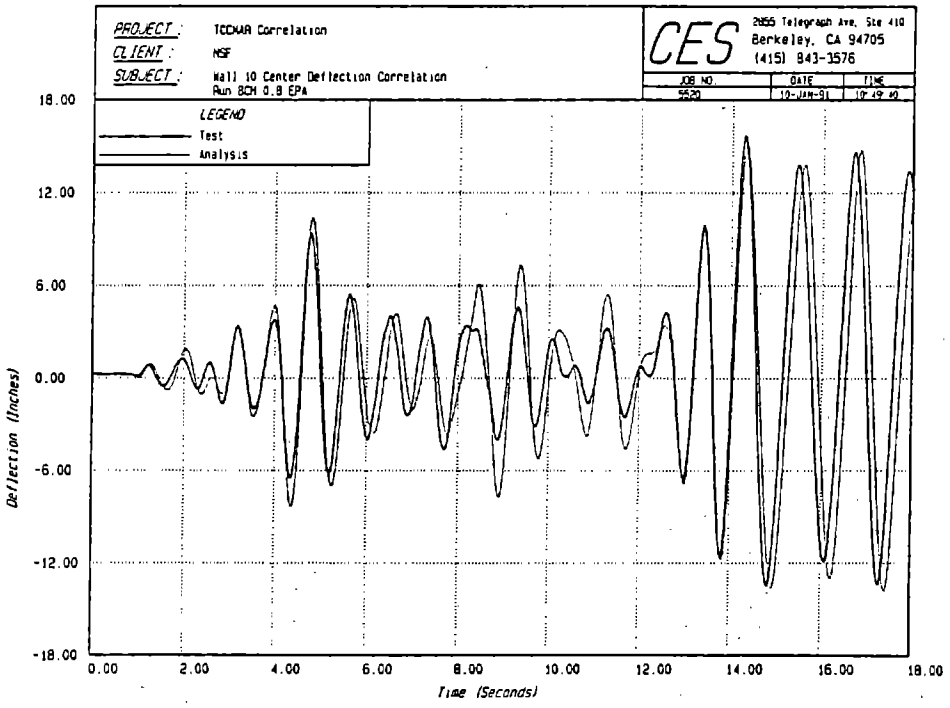

Figure 38: Comparison of Test and Analytical Deflections - Wall 10 Run BCH

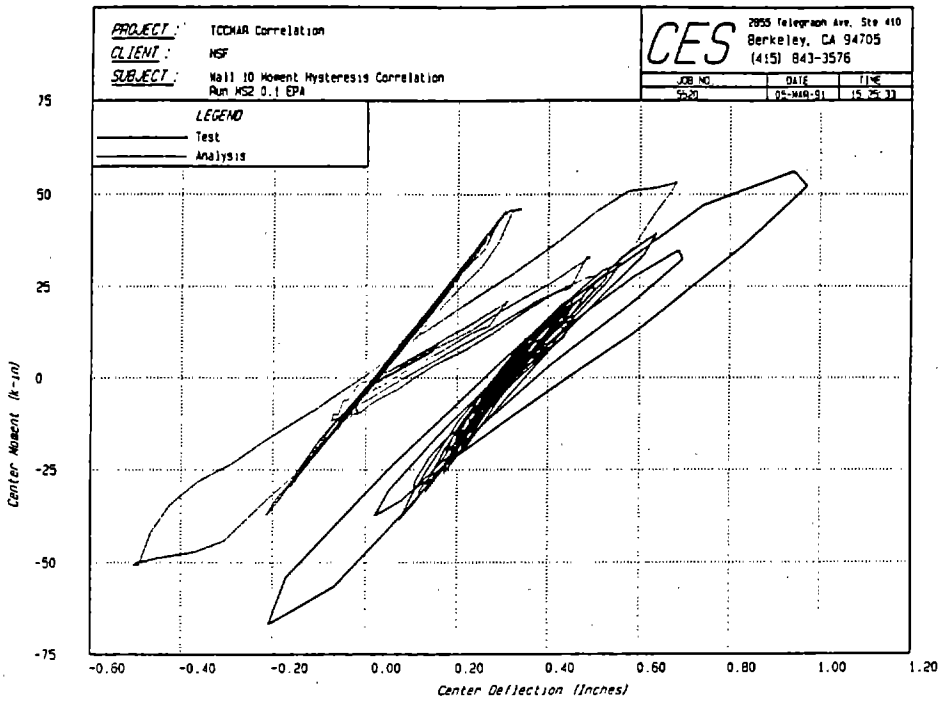

Figure 39: Comparison of Test and Analytical Hysteresis Loops - Wall 10 Run MS2 (Offset = 0.25")

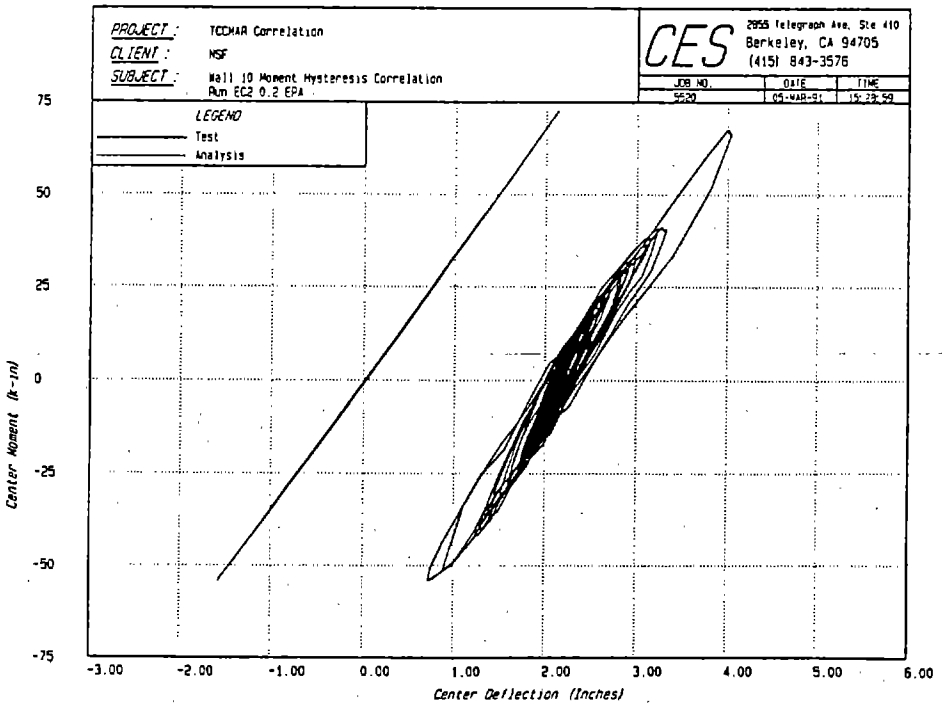

Figure 40: Comparison of Test and Analytical Hysteresis Loops - Wall 10 Run EC2 (Offset = 2")

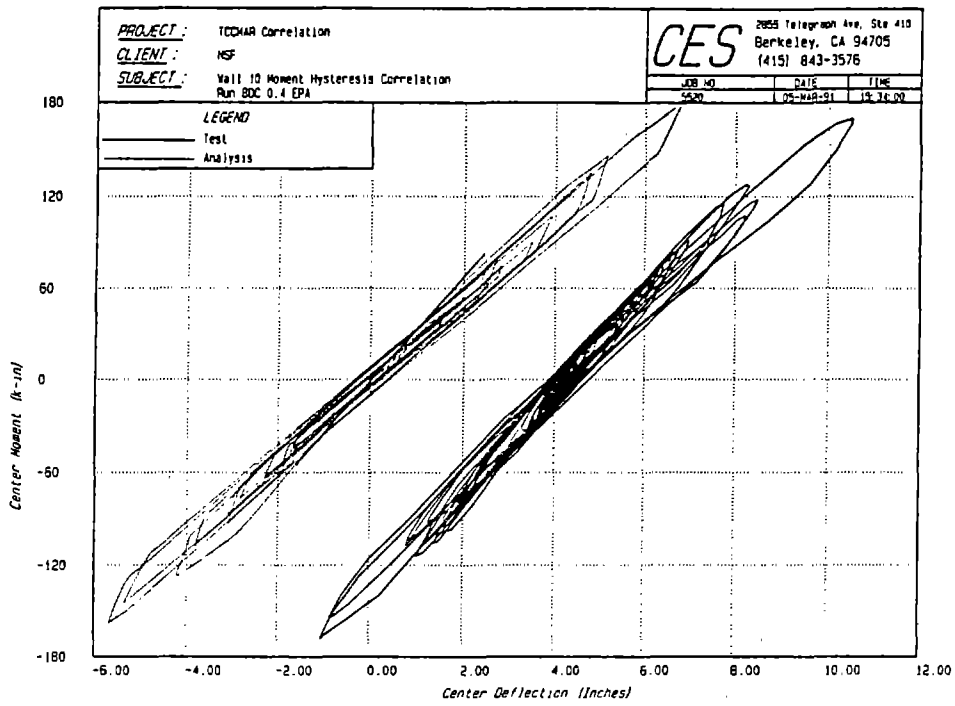

Figure 41: Comparison of Test and Analytical Hysteresis Loops - Wall 10 Run BDC (Offset = 4")

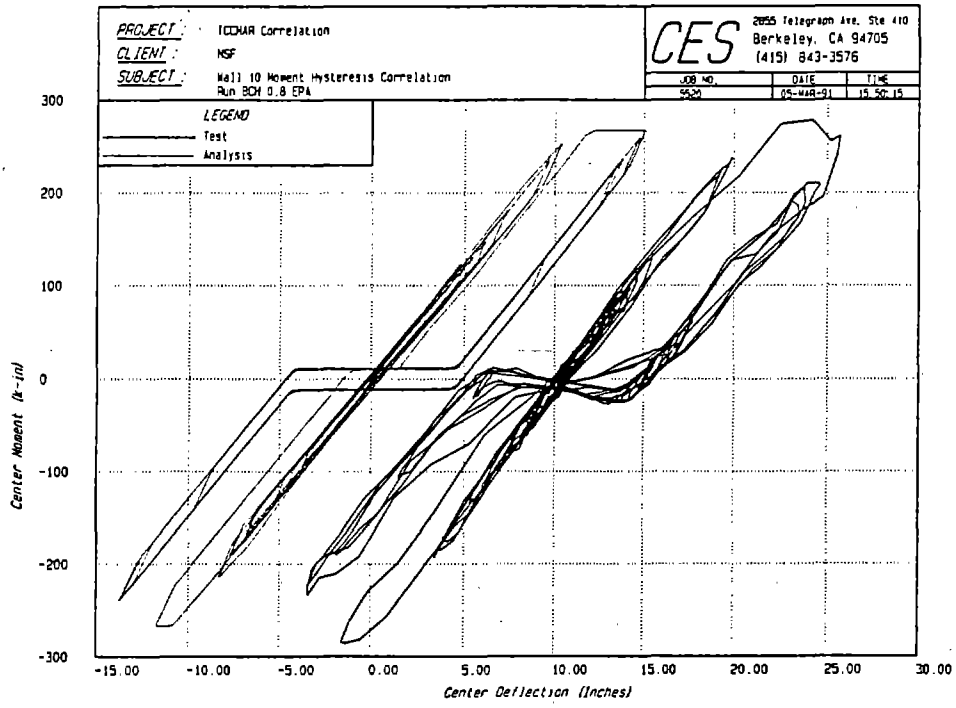

Figure 42: Comparison of Test and Analytical Hysteresis Loops - Wall 10 Run BCH (Offset = 10")

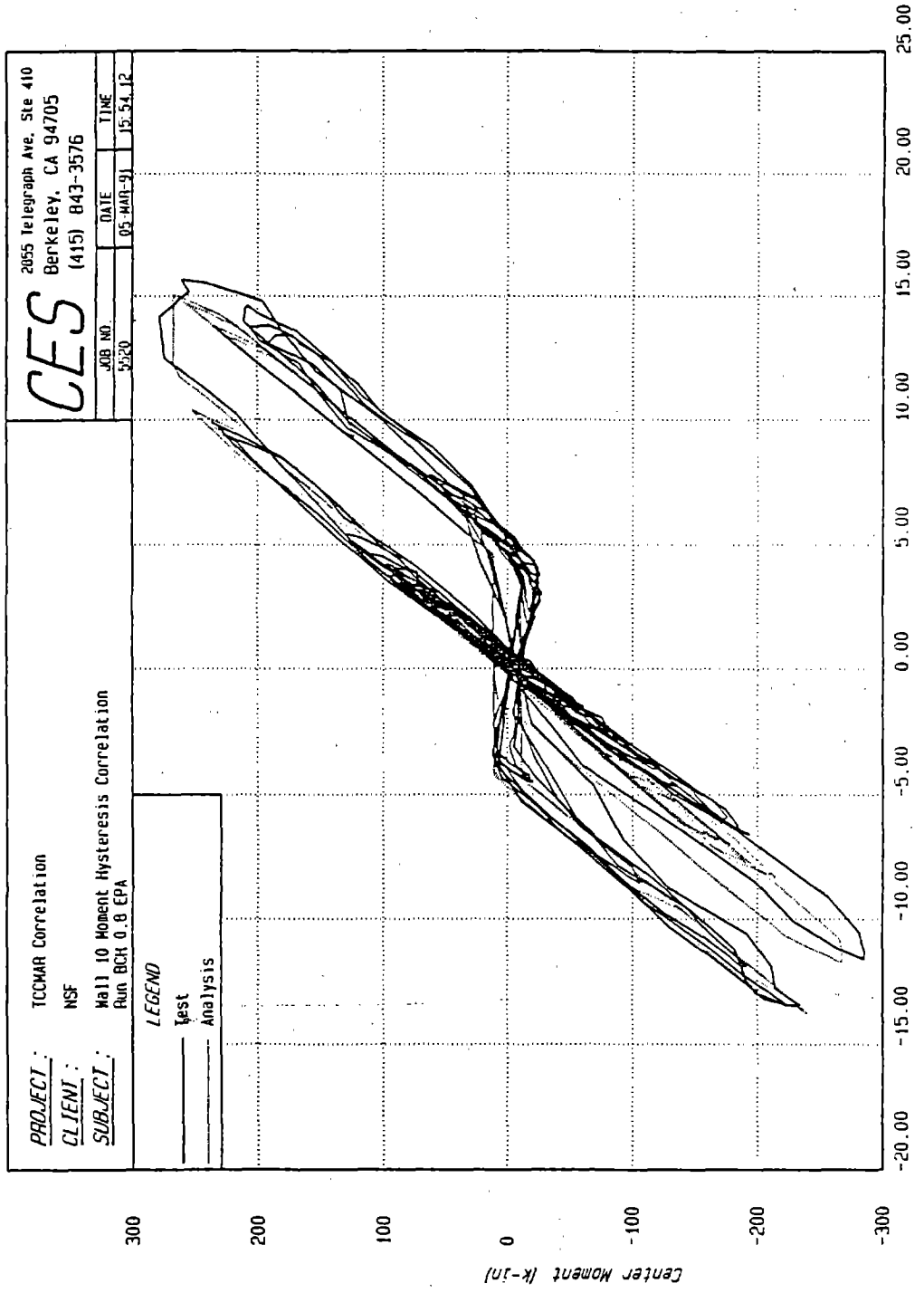

Figure 43: Comparison of Test and Analytical Hysteresis Loops - Wall 10 Run BCH
(No Offset)

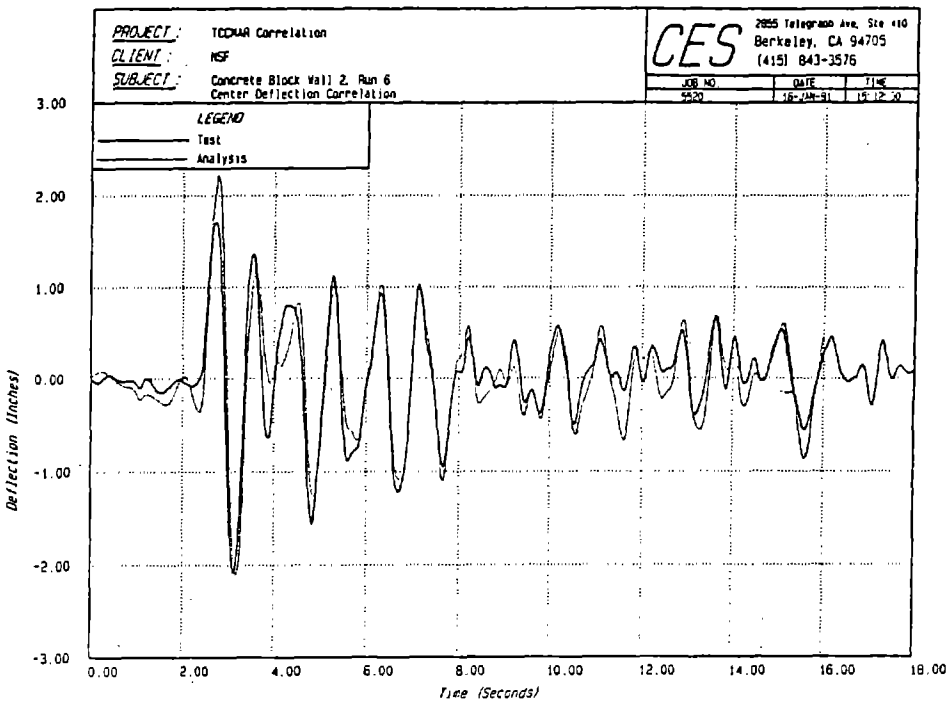

Figure 44: Comparison of Test and Analytical Deflections - Block Wall 2 Run 6

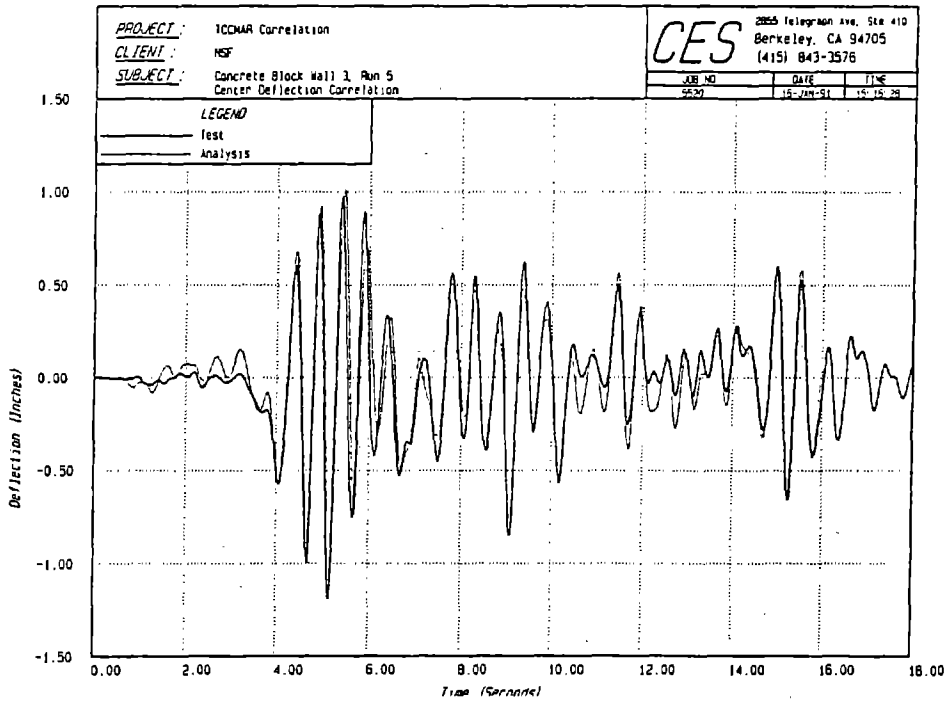

Figure 45: Comparison of Test and Analytical Deflections - Block Wall 3 Run 5

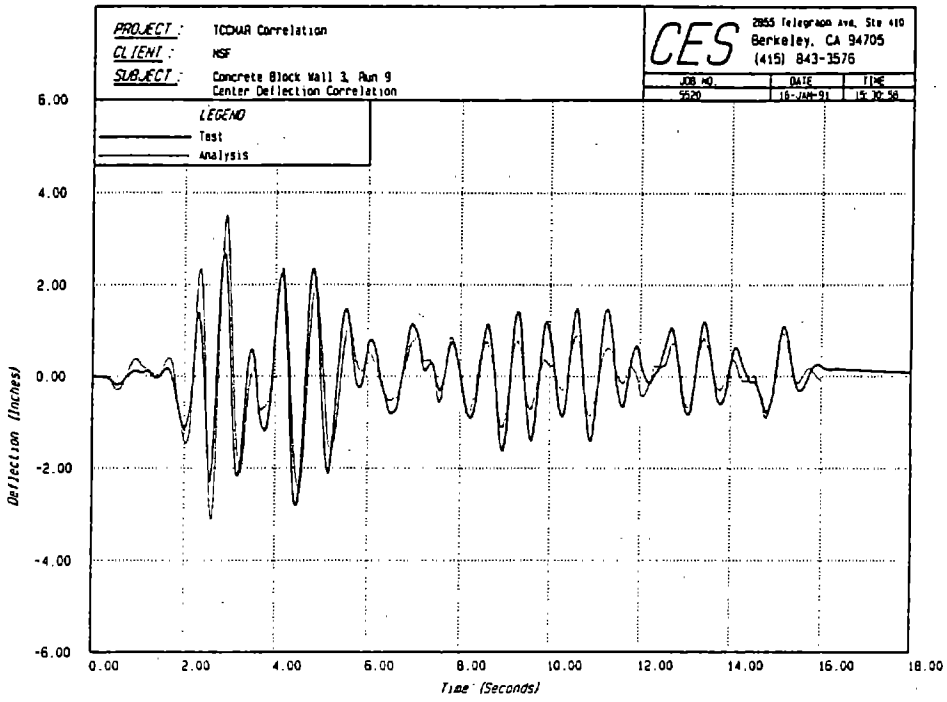

Figure 46: Comparison of Test and Analytical Deflections - Block Wall 3 Run 9

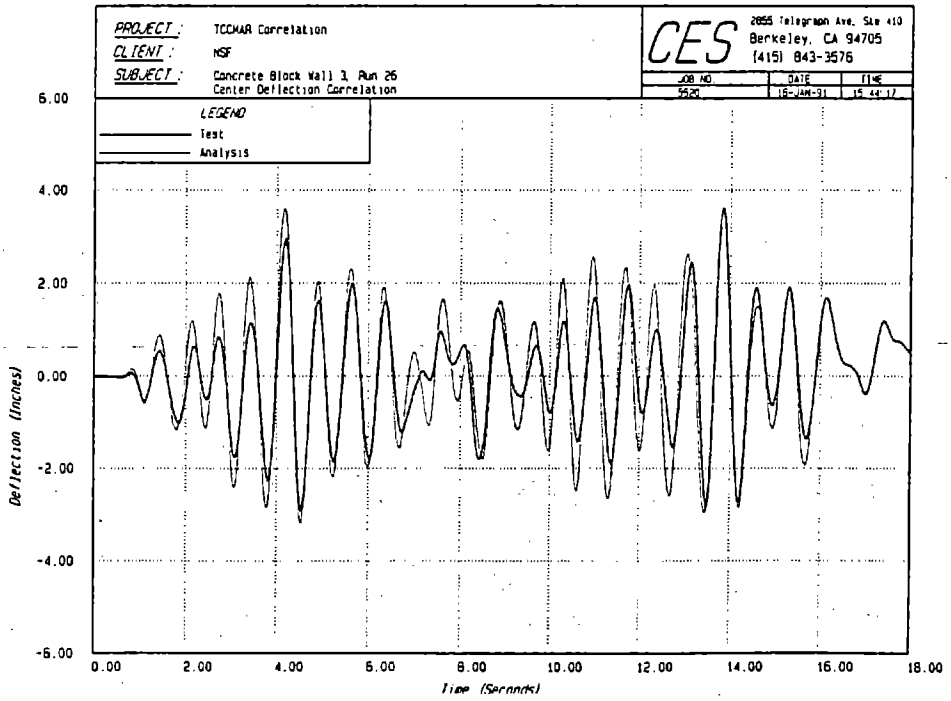

Figure 47: Comparison of Test and Analytical Deflections - Block Wall 3 Run 26

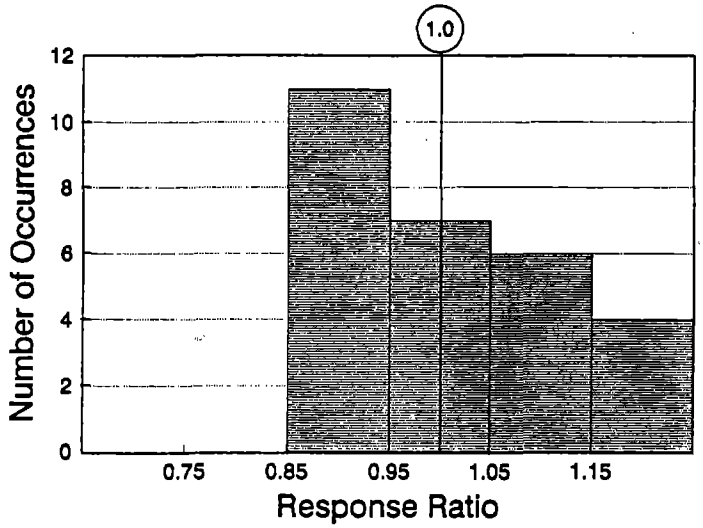

(a) Deflection

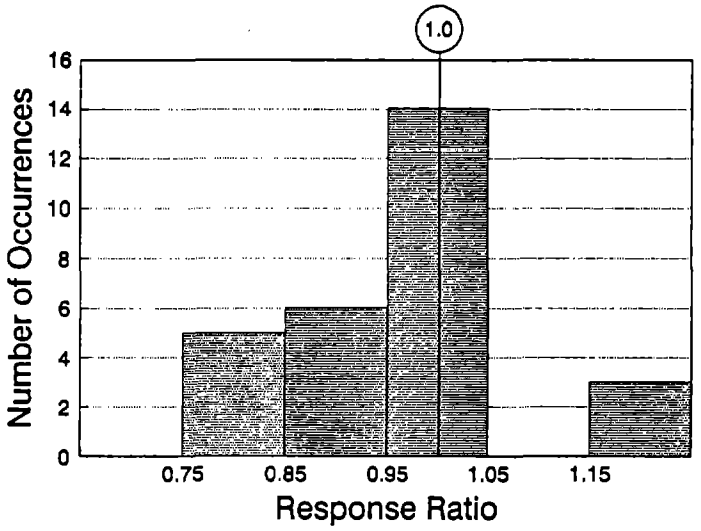

(b) Moment

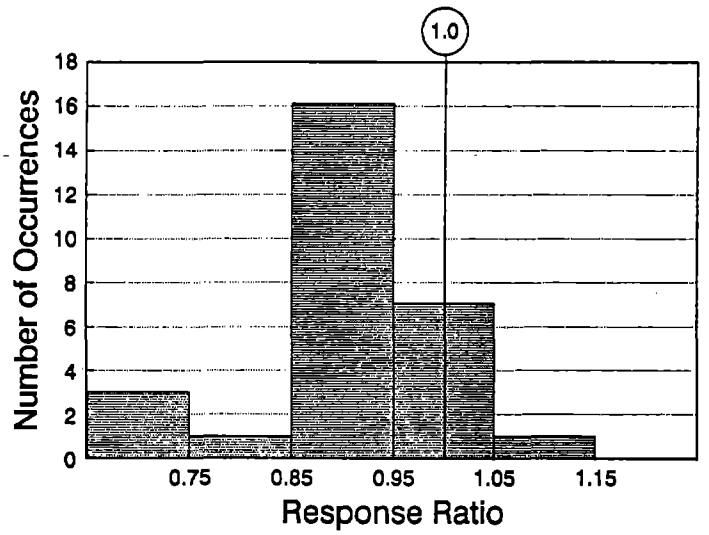

(c) Reaction

Figure 48: Histograms of Response Ratios

5 Summary and Conclusions

This report has described the development of an analytical model to predict the out-of-plane seismic response of reinforced masonry walls. It has further described the correlation of analytical results from the model with measurements taken during two full-scale dynamic test programs, one on clay brick walls, the other on concrete block walls.

The analytical model consists of a series of elastic flexural line elements with inelastic hinges at their ends. A typical wall is modelled by six such elements over its height. For fixed-base walls, a base hinge is permitted to form. An inelastic hinge is permitted to form at only one place within the wall height: the location where the wall first cracks. All subsequent inelastic behavior is confined to that location. The inelastic hysteretic properties of the hinge have been empirically derived to match the observed moment-deflection hysteresis loops from the clay brick test program. The user describes a wall in terms of its physical properties, so that the empiricism is transparent. A small displacement formulation has been adopted, with geometric stiffness used to represent the destabilizing effects of compressive loads on the wall. Such a formulation provides a numerically efficient representation of actual wall behavior.

The model is excited by kinematic motion histories at its top and base. These motions must be derived independently of the wall analysis: in other words, the current model does not capture any interaction between an out-of-plane wall and the remainder of the structure. In the language of the TCCMAR project, this is a Structural Component Model (SCM).

The ability of the model to predict the seismic response of real walls has been tested by subjecting the model to top and bottom motions as recorded during the two full-scale dynamic test programs. In the case of clay brick walls, seven distinct wall models are each subjected to a standard series of twelve dynamic motions. In the case of concrete block walls, two wall models are subjected to a total of four recorded dynamic motions. A critical evaluation of the results from these analyses indicates that they closely match the corresponding test results for a considerable range of wall parameters and input motion levels.

Three measures of response have been used for correlation purposes: midheight relative deflection, midheight moment, and total (sum of top and bottom) reaction. For two selected clay brick walls, results from individual runs are presented, and the analytical response history traces are compared to those measured. For the remaining walls, only maxima are compared. Deflection response is predicted very well: over all walls, the mean response ratio (analytical response divided by measured response) is 1.0. For moment response, the mean response ratio is 0.96, while for reaction, the mean response ratio is 0.90. In each case, the coefficient of variation is about 10%. Thus, deflections are best predicted, with moments and reactions slightly less well predicted. However, all quantities are predicted with sufficient accuracy to have confidence in the model.

The discrepancies for moment and reaction can be understood by considering the deflected shape that is permitted in the analysis: on either side of the inelastic hinge there are elastic flexural elements with a stiffness corresponding to an uncracked wall. Thus, the analytical

shape tends towards two straight lines, with nearly all the rotation concentrated at a single point (the inelastic hinge). In real walls, the cracking and corresponding softening occurs over a significant height within the wall, with the result that rotation is spread over a wide region, and the deflected shape is much "softer" than the analytical shape. The analytical model thus underestimates the displacements and accelerations at points in the wall away from the point of maximum deflection. Thus the corresponding inertia forces in the analysis are underestimated, with the result that the moments and reactions are less well predicted than the deflections. However, the loss of accuracy in moments (average 4%) and reactions (average 10%) is not considered serious.

The correlation results reported herein were obtained using the hysteretic damping explicitly included in the inelastic hinge, with an additional viscous component. A value of 1% of critical was necessary to achieve the reported correlation. Depending on wall properties, the equivalent viscous damping for the hysteretic action is in the range of 3% to 6% of critical. Thus one conclusion from the correlation effort is that realistic values of damping for reinforced masonry walls responding out-of-plane lies between 4% and 7% of critical. This is generally consistent with other reported values, and with the state of practice in the earthquake engineering community.

One very interesting and important feature of wall response was clearly apparent during the correlation exercise: the sensitivity of response to the initial state of the wall before the application of a particular motion. An analysis of a previously damaged wall is achieved by specifying a previous maximum deflection that the wall has experienced. It has been demonstrated that the subsequent response can be very sensitive to the chosen value. This phenomenon is perhaps most important in regions of low seismic activity, where a visibly undamaged wall may in fact have been previously cracked. These analyses have demonstrated that the subsequent response including and ignoring the previous damage could change by a factor of up to 5. Such changes in response are also clearly apparent in the test results. For example, compare the response of walls 10 (0.47 inches) and 11 (2.14 inches) to run MS1. The only difference is that wall 11 has spliced rebars, which is demonstrated by the test program to have a generally negligible effect. Thus one concludes that the difference in response is due to wall 11 being precracked for run MS1. At higher seismic inputs, the effect is also present. This is demonstrated in the correlations for walls 4 and 6 which used a non-standard order for the test motions. The response changes by a factor of about 2 at the 0.4 EPA level when the standard order rather than the test order is used in the analysis.

A forthcoming companion report will focus on a parameter study which is designed to extend the range of wall properties studied in the laboratory specimens. Thus no attempt has been made in this report to discuss the impact of several key wall parameters on wall response.

Based on the correlation reported herein, the analytical model can be used with confidence to perform the parameter study. It can also be used by designers to compute realistic out-of-plane responses for their walls, and thus engineer safer and more serviceable masonry structures in seismic regions.

6 References

[1] Blondet, M. and Mayes, R.L., "The Transverse Response of Clay Masonry Walls Subjected to Strong Motion Earthquakes: Summary of Dynamic Test Results," (in 4 Volumes), Report No. 3.2(b2)-D, U.S.-Japan Coordinated Program for Masonry Building Research, April 1991.

[2] Sveinsson, B.I., Blondet, M. and Mayes, R.L., "The Transverse Response of Clay Masonry Walls Subjected to Strong Motion Earthquakes - Report on the Testing of Wall No. 10," Report No. 3.2(b2)-10, U.S.-Japan Coordinated Program for Masonry Building Research, December 1988.

[3] Agbabian, M.S., Adham, S.A., Masri, S.F., Avanessian, V. and Traina, I., "Out-of-Plane Dynamic Testing of Concrete Masonry Walls (Volume I: Final Report, Volume II: Test Results)," Report No. 3.2(b1), U.S.-Japan Coordinated Program for Masonry Building Research, July 1989.

[4] "Test Report on Slender Walls," ACI-SEASC Task Committee on Slender Walls, Los Angeles, California, February 1980 - September 1982.

[5] Blondet, J.M., Mayes, R.L. and Kelly, T.E., "Out-of-Plane Testing of Slendor Hollow Clay Masonry Block Walls," Proceedings, The Fifth North American Masonry Conference, Illinois, June 1990.

[6] Mondkar, D.P. and Powell, G.H., "ANSR-II: Analysis of Nonlinear Structural Response, User's Manual," Report No. UCB/EERC 79/17, Earthquake Engineering Research Center, University of California, Berkeley, California, July 1979.

[7] Clough, R.W. and Penzien, J., Dynamics of Structures, McGraw-Hill, New York, 1975.

[8] Ewing, R.D, Kariotis, J.C. and El-Mustapha, A., "LPM/I: A Computer Program for the Nonlinear, Dynamic Analysis of Lumped Parameter Models," Report No. 2.3-1, U.S.-Japan Coordinated Program for Masonry Building Research, August 1987.

[9] Blondet, M. and Mayes, R.L., "The Transverse Response of Clay Masonry Walls Subjected to Strong Motion Earthquakes: Summary of Static Test Results," Report No. 3.2(b2)-S, U.S.-Japan Coordinated Program for Masonry Building Research, 1991.

WALLY may be run in either interactive input or batch input mode. If the program is operated in batch mode, then an input file needs to be prepared using any text editor. Alternatively, running **WALLY** in interactive mode once will automatically create an input file which can be subsequently edited and used with future batch runs. All information in an input file is free format, and "comment" lines can be inserted in the file at any location by using an exclamation point ("!") in column one of that line. A sample input file follows, together with a line-by-line description of the data. Note that the main input file references a second input file containing a description of the support motions. This support motion file is described subsequently.

Sample Input File

Line numbers are not part of the actual input file but rather are used here for reference purposes. Only the data lines are described below. The comment lines are used to readily identify the data fields for use with a text editor.

line

```
 1 Wall 10 correlation study - run BDC
 2 ! height  thickness  self weight   grout      prior defl
 3    300.       5.5         58.      partial        3.0
 4 ! rebar #   spacing   # splices   ht 1   len 1   ht 2   len 2
 5     7          16          2        80      40     180     40
 6 !  f'm        fr         fy
 7   4900.      200.       62.8
 8 ! top support  bottom support    # elements    analysis
 9      pin            pin               6        support
10 ! static loads at top of wall
11 !  vertical load       eccentricity
12         0.3                -8.
13 Top and base support motion measured in the test program
14 indis.bc
15 ! time step      # steps     damping
16     0.01          2000        0.01
```

Description of Input File

Line 1 **Problem title** used in headers on output file pages.
(maximum 72 characters)

Line 3 **Physical description of the wall.** This line should contain the following information:

Field	Entry	Units / Description
1	wall height	inches
2	block thickness	inches
3	self weight of wall	lb/ft^2
4	grouting	'full' or 'partial'
5	prior max. deflection	inches

Line 5 **Description of vertical reinforcement.** This line should contain the following information:

Field	Entry	Units / Description
1	vertical rebar size	#
2	vertical rebar spacing	inches
3	number of splices	maximum is 2
4	height of splice 1	inches
5	length of splice 1	inches
6	height of splice 2	inches
7	length of splice 2	inches

Notes:

- Omit fields 4 through 7 if there are no splices.
- Omit fields 6 and 7 if there is one splice.
- The program only handles splices placed symmetrically with respect to the wall height.
- Height is measured from the base of the wall to the bottom of the splice.

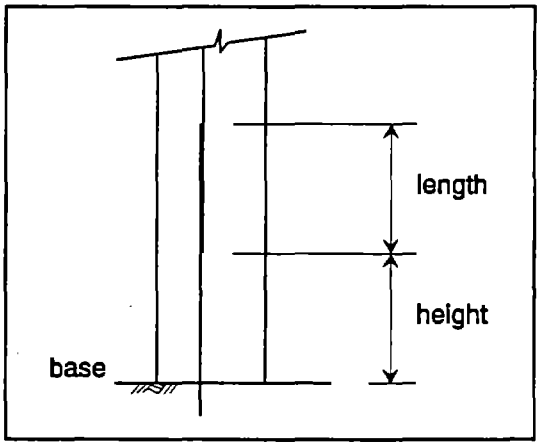

Line 7 **Material property description.** This line should contain the following information:

Field	Entry	Units
1	masonry cube strength f'_m	psi
2	mortar modulus of rupture f_r	psi
3	yield strength of steel rebar f_y	ksi

Line 9 **Modelling information.** This line should contain the following:

Field	Entry	Description
1	top support	must be 'pin'
2	bottom support	'pin' or 'fixed'
3	number of elements up wall height	2, 4, 6 or 8
4	analysis type	'support'

Line 12 **Vertical static load description.** This line should contain the following information:

Field	Entry	Units / Description
1	vertical load	k/ft (compression +)
2	eccentricity	inches

Line 13 **Title for dynamic analysis** (maximum 72 characters)

Line 14 **Name of file containing support motions**
(may include a path - for example
`c:\walls\motions\shake1.dat`)

Line 16 **Dynamic analysis parameters.** This line should contain the following information:

Field	Entry	Units / Description
1	time step	seconds
2	number of time steps	maximum is 4000
3	damping	fraction of critical typically 0.01

Note: The damping supplied here is viscous damping. The hysteretic damping is automatically included in the element formulation.

Sample Support Motion Input File

The following is part of a typical support motion file. Note that the single input file contains information on **both** the base and top support motions. A description of the contents follows the listing of the file.

```
Base displacement history - run BDC                          (6f10.4)
   5002      1      .0040     2000       1.00
     .1908      .1900      .1892      .1886      .1881      .1880
     .1880      .1880      .1881      .1880      .1878      .1874
     .1871      .1866      .1864      .1864      .1866      .1871
     .1876      .1882      .1886      .1890      .1892      .1891
     .
     .
     .
Top displacement history - run BDC                           (6f10.4)
   5002      1      .0040     2000       1.00
     .1720      .1721      .1726      .1734      .1742      .1750
     .1756      .1760      .1759      .1753      .1742      .1731
     .1717      .1704      .1693      .1687      .1683      .1683
     .1688      .1694      .1703      .1712      .1721      .1729
     .
     .
     .
```

Description of Support Motion Input File

The base motion should be described first, followed by a similar description of the top motion. Motions may be described by displacements, velocities or accelerations. **WALLY** uses displacements for its computations, so if velocities or accelerations are input, they will be integrated prior to analysis. For this reason, if velocity or acceleration histories are specified, care should be taken to provide sufficient significant digits in the histories and a sufficiently fine input time step so that meaningful displacements will result from the integration. Zero initial conditions are assumed for displacements and velocities.

In a typical application for a single story commercial structure (such as a gymnasium or warehouse), the base motion will be a recorded or artificially generated ground motion, and the top motion will be computed as the diaphragm motion at the level of the top of the wall, when the base motion excites a mathematical model of the structure.

Line 1 Supply the following information:

Columns	Entry
1-60	title for support motion
61-80	format for motion history

Line 2 Supply the following information:

Field	Entry	Units / Description
1	number of input points	maximum is 8000
2	input motion code	1 for displacement 2 for velocity 3 for acceleration
3	input time step	seconds
4	number of interpolated points (at analysis time step)	maximum is 4000
5	scale factor for motion	typically 1.0 or 386.4

Subsequent lines Input motions in the format described on line 1.

Repeat the entire sequence for top support motion as indicated in the sample motion file above.